

Efficient Computation of Pareto Optimal Beamforming Vectors for the MISO Interference Channel with Successive Interference Cancellation

Johannes Lindblom, *Student Member, IEEE*, Eleftherios Karipidis, *Member, IEEE*,
and Erik G. Larsson, *Senior Member, IEEE*

Abstract—We study the two-user multiple-input single-output (MISO) Gaussian interference channel where the transmitters have perfect channel state information and employ single-stream beamforming. The receivers are capable of performing successive interference cancellation, so when the interfering signal is strong enough, it can be decoded, treating the desired signal as noise, and subtracted from the received signal, before the desired signal is decoded. We propose efficient methods to compute the Pareto-optimal rate points and corresponding beamforming vector pairs, by maximizing the rate of one link given the rate of the other link. We do so by splitting the original problem into four subproblems corresponding to the combinations of the receivers' decoding strategies - either decode the interference or treat it as additive noise. We utilize recently proposed parameterizations of the optimal beamforming vectors to equivalently reformulate each subproblem as a quasi-concave problem, which we solve very efficiently either analytically or via scalar numerical optimization. The computational complexity of the proposed methods is several orders-of-magnitude less than the complexity of the state-of-the-art methods. We use the proposed methods to illustrate the effect of the strength and spatial correlation of the channels on the shape of the rate region.

Index Terms—Beamforming, interference channel, interference cancellation, multiple-input single-output (MISO), Pareto boundary, Pareto optimality, rate region.

I. INTRODUCTION

We study a wireless system where two adjacent transmitter (TX) – receiver (RX) pairs, or links, operate simultaneously in the same frequency band and interfere with each other. Each TX employs $n_T > 1$ antennas, whereas each RX is equipped with a single antenna. Hence, the system is modeled as the so-called multiple-input single-output (MISO) interference channel (IC) [3]. We assume that the TXs have perfect knowledge of the local channels to both RXs and use

scalar Gaussian codes followed by single-stream beamforming. Also, we assume that the RXs are capable to perform successive interference cancellation (SIC) [4]. That is, when the interfering signal is strong enough¹, a RX can decode it and subtract it from the received signal before decoding the desired signal. The decoding is done independently, since the RXs are located apart and there is no coordination amongst them. SIC capability is an important assumption because in principle it leads to higher achievable rates than in case where the RXs treat interference as noise. Note that the SIC rate region is a superset of the region achieved when interference is treated as noise, since the latter is a special case of the former. We see this by noting that the optimal decoding process might be to directly decode the intended signal treating the interference as noise. Once the intended signal is decoded, the RXs are not interested in decoding the interference. The resulting achievable rate region is defined by the so-called Pareto boundary, which is the set of points where the rate of one link cannot increase without decreasing the rate of the other.

The objective of this paper is to propose computationally efficient methods for finding, in a centralized way, the Pareto-optimal (PO) pairs of beamforming vectors which yield operating points on this Pareto boundary. These methods are important because they enable a fast computation of the rate region. Hence, we can use them to illustrate how different channel realizations affect the shape of the rate region or in the context of large-scale simulation studies of interference networks. Moreover, they provide valuable insight on the beamforming design and inspiration for practical implementations.

The capacity region of the IC is in general unknown, but it is known for certain cases. For strong interference, the capacity region coincides with the capacity region for the case where both RXs decode both messages, i.e., it is the intersection of the capacity regions of two multiple-access channels, see [5]–[7]. For weak interference it is optimal to treat it as noise, see [8] for the single-antenna IC and [9] for the multi-antenna IC. For the MISO IC, various achievable rate regions have been proposed and studied, e.g., in [10]–[14]. Especially, the case of treating interference as noise has been the subject of intense studies, e.g., in [13]–[20]. In [17], it was shown that single-stream beamforming is optimal for Gaussian codes. In [13], a parameterization of the PO beamforming

Manuscript received October 6, 2012; revised March 22, 2013 and May 31, 2013; accepted June 10, 2013. This work has been supported in part by the Swedish Research Council (VR), the Swedish Foundation of Strategic Research (SSF), and the Excellence Center at Linköping-Lund in Information Technology (ELLIIT). This work has been performed in the framework of the European research project SAPHYRE, which was partly funded by the European Union under its FP7 ICT Objective 1.1 - The Network of the Future. Preliminary versions of parts of the material in this paper were presented at ICASSP'11 [1] and CAMSAP'11 [2].

J. Lindblom and E. G. Larsson are with the Communication Systems Division, Department of Electrical Engineering (ISY), Linköping University, SE-581 83 Linköping, Sweden (e-mail: {lindblom,erik.larsson}@isy.liu.se).

E. Karipidis was with the Communication Systems Division, Department of Electrical Engineering (ISY), Linköping University, SE-581 83 Linköping, Sweden. He is now with Ericsson Research, Stockholm, Sweden (e-mail: karipidis@ieee.org).

¹In Sec. III, we explain what mean by strong enough in the current context.

vectors was proposed based on the properties that they use full transmit power and lie in the subspace spanned by the local channels. Alternative parameterizations were proposed in [15] and [14], using the concepts of virtual signal-to-interference-plus-noise ratio (SINR) and gain regions, respectively. In [21], the rate region for the related scenario of cooperative multicell precoding was characterized. The parameterizations for the two-user MISO IC illustrate that for any number of transmit antennas, it can be reduced to an equivalent MISO IC where each TX has two antennas [9].

The MISO IC with SIC-capable RXs was investigated in [22] where the gain potential of SIC over treating interference as noise was illustrated in terms of average rate at a Nash equilibrium. Later, in [11], the achievable rate region for SIC-capable RXs was formalized and in [12] a parameterization for the PO beamforming vectors was proposed, extending the respective result of [13]. A related work appears in [10], where a simplified version of the Han-Kobayashi region [6] was studied and semidefinite relaxation was used to propose power control schemes and compute the corresponding rate region.

The parameterizations in [13] and [12] are useful analytical tools and they enable a better intuitive understanding of the properties of the PO beamforming vectors. When the RXs treat interference as noise, the PO beamforming vectors are obtained by trading off between the conflicting objectives of maximizing the desired signal power and minimizing the interference [13]. For SIC capable RXs, the trade-off is between maximization of the desired signal power and maximization of the interference, to enable SIC [12]. Another merit of these parameterizations is that they substantially decrease the dimension of the search space for a PO beamforming vector, from n_T complex variables to one or two nonnegative real variables. However, besides the dimensionality reduction, these parameterizations do not directly provide a method for efficient computation of the Pareto boundary. The reason is that they only constitute *necessary* conditions that the beamforming vector of each TX has to *separately* fulfill, whereas it is *pairs* of beamforming vectors that yield PO operating points. The state-of-the-art use of the parameterizations has been to sample the parameters, consider all possible combinations to generate a large number of achievable rate pairs, and perform a brute-force search amongst them to find the ones comprising the Pareto boundary, e.g., see [13].

It is desirable to devise a method which directly and efficiently computes PO points. Joint optimization of the beamforming vectors is required for this purpose. As shown in [18], the problem of jointly maximizing a common utility function and of finding PO points is NP-hard in general. Nevertheless, several methods have been recently proposed, e.g., [16] and [23], which apply successive convex optimization techniques on the vector space of the beamforming vectors to find the Pareto boundary when the RXs treat interference as noise. The methods proposed herein achieve much higher computational efficiency by optimizing instead on the parameter space which characterizes the PO beamforming vectors of the SIC region. For the case of treating interference as noise, this was attempted in [24], where monotonic optimization was used to find specific PO points, e.g., the maximum sum-rate point. The

method proposed therein was faster than a brute-force search, but far less efficient than the methods we propose.

A. Contributions and Organization

In Sec. II, we give the system model. In Sec. III, we define the SIC achievable rate region and formulate the optimization problem that yields an arbitrary point on the Pareto boundary, as a maximization of the rate of one link given the rate achieved by the other link. In Sec. IV–VI, we propose very efficient methods to solve this problem, by combining, unifying, and improving the preliminary approaches that appeared in our conference contributions [1] and [2]. The common denominator of these methods is to exploit the parameterizations and equivalently recast the maximization problem so that it can be solved analytically or via scalar optimization. The proposed method is applied on the following regions, whose union constitutes the SIC region:

1) In Sec. IV, we propose two methods to find the region where both RXs treat the interference as noise. In the first method, we equivalently formulate the originally non-concave rate maximization problem as a scalar quasi-concave problem, which we solve optimally with a gradient search approach. To find the Pareto boundary, we repeat this optimization for various choices of the input rate. This method is novel and improves the one in [23] in two ways: a) we reduce the feasible set significantly from the set of beamforming vectors to the parameter set defined in [13] and b) we solve a single quasi-concave optimization problem instead of a sequence of convex feasibility problems. In the second method, we use the KKT conditions to derive a closed-form relation that couples the parameters of the TXs yielding a PO pair. To find the Pareto boundary, we repeatedly solve the cubic equation resulting from various choices for one of the parameters. This method was presented in [1]; herein we give in addition a formal proof of global optimality of all solutions to the KKT conditions. A similar result was independently derived in [19] and later extended in [20]. However, [19] and [20] did not prove that all feasible solutions to the corresponding cubic equation are global optima and potentially they discard optimal solutions.

2) In Sec. V, we find the two regions where one RX decodes the interference, before decoding the desired signal, while the other treats the interference as noise. We use the parameterization of [11] to equivalently recast the rate maximization problem as a quasi-concave problem of three real variables and determine the solution in closed-form. This method was presented in [2]; herein, we give in addition a more detailed derivation of the result.

3) In Sec. VI, we find the region where both RXs decode the interference. We use the parameterization of [11] and split the rate maximization problem in two quasi-concave scalar subproblems. This method improves the corresponding one in [2] in two ways: a) the number of variables is decreased from four real variables to a single one and b) a single instance of each of the two quasi-concave subproblems needs to be solved instead of a sequence of convex feasibility problems.

In Sec. VII, we provide illustrations of the rate regions for different channel properties and a complexity analysis. In Sec. VIII, we make some concluding remarks.

The source code that implements the proposed methods and generates the illustrations in Sec. VII is available at <http://urn.kb.se/resolve?urn=urn:nbn:se:liu:diva-93845>.

B. Notation

Boldface lowercase letters, e.g., \mathbf{x} , denote column vectors. $\{\cdot\}^H$ denotes the Hermitian (complex conjugate) transpose of a vector. The Euclidean norm of a vector \mathbf{x} is denoted $\|\mathbf{x}\|$. By $x \sim \mathcal{CN}(0, \sigma^2)$ we say that x is a zero-mean complex-symmetric Gaussian random variable with variance σ^2 . We denote the orthogonal projection onto the space spanned by the vector \mathbf{x} as $\mathbf{\Pi}_{\mathbf{x}} \triangleq \mathbf{x}\mathbf{x}^H / \|\mathbf{x}\|^2$. The orthogonal projection onto the orthogonal complement of \mathbf{x} is $\mathbf{\Pi}_{\mathbf{x}}^\perp \triangleq \mathbf{I} - \mathbf{\Pi}_{\mathbf{x}}$, where \mathbf{I} is the identity matrix. Note that for a vector \mathbf{y} , we have $\|\mathbf{y}\|^2 = \|\mathbf{\Pi}_{\mathbf{x}}\mathbf{y}\|^2 + \|\mathbf{\Pi}_{\mathbf{x}}^\perp\mathbf{y}\|^2$. We let $f'(x)$ and $f''(x)$ denote the first and second derivatives, respectively, of a function $f(x)$. We define $[x]_{\bar{x}} \triangleq \max\{\underline{x}, \min\{x, \bar{x}\}\}$.

II. SYSTEM MODEL

We assume that the transmissions consist of scalar coding followed by single-stream (rank-1) beamforming and that all propagation channels are frequency-flat. The matched-filtered symbol-sampled complex baseband signal received by RX $_i$ is then modeled as

$$y_i = \mathbf{h}_{ii}^H \mathbf{w}_i s_i + \mathbf{h}_{ji}^H \mathbf{w}_j s_j + e_i, \quad i, j \in \{1, 2\}, \quad j \neq i. \quad (1)$$

In (1), $\mathbf{h}_{ji} \in \mathbb{C}^{n_T}$ is the (conjugated) channel vector for the link TX $_j \rightarrow$ RX $_i$. We assume that TX $_i$ perfectly knows the direct and crosstalk channels, \mathbf{h}_{ii} and \mathbf{h}_{ij} , respectively, and that these are neither co-linear nor orthogonal. Also, $\mathbf{w}_i \in \mathbb{C}^{n_T}$ is the beamforming vector employed by TX $_i$, $s_i \sim \mathcal{CN}(0, 1)$ is the transmitted symbol of TX $_i$, and $e_i \sim \mathcal{CN}(0, \sigma_i^2)$ models the thermal noise at RX $_i$. The TXs have power constraints that we, without loss of generality, set to 1 and define the set of feasible beamforming vectors as $\mathcal{W} \triangleq \{\mathbf{w} \in \mathbb{C}^{n_T} \mid \|\mathbf{w}\|^2 \leq 1\}$. The achievable rate for RX $_i$ depends on the received powers

$$p_i(\mathbf{w}_i) \triangleq |\mathbf{h}_{ii}^H \mathbf{w}_i|^2 \quad \text{and} \quad q_i(\mathbf{w}_j) \triangleq |\mathbf{h}_{ji}^H \mathbf{w}_j|^2 \quad (2)$$

over the direct and crosstalk channel, respectively.

In order to simplify the subsequent notation, we define the following channel-dependent constants. We define $g_{ij} \triangleq \|\mathbf{h}_{ij}\|$ and $\kappa_i \triangleq |\mathbf{h}_{ij}^H \mathbf{h}_{ii}| / (\|\mathbf{h}_{ij}\| \|\mathbf{h}_{ii}\|)$, $j \neq i$. The latter is the cosine of the Hermitian angle between \mathbf{h}_{ii} and \mathbf{h}_{ij} . When $\kappa_1 = 1$ or $\kappa_1 = 0$ the channels are parallel or orthogonal, respectively. Then, using these constants, we define

$$\alpha_i \triangleq \|\mathbf{\Pi}_{\mathbf{h}_{ij}} \mathbf{h}_{ii}\| = g_{ij} \kappa_i, \quad j \neq i, \quad (3)$$

$$\tilde{\alpha}_i \triangleq \|\mathbf{\Pi}_{\mathbf{h}_{ij}}^\perp \mathbf{h}_{ii}\| = \sqrt{g_{ij}^2 - \alpha_i^2} = g_{ij} \sqrt{1 - \kappa_i^2}, \quad j \neq i, \quad (4)$$

$$\beta_i \triangleq \|\mathbf{\Pi}_{\mathbf{h}_{ii}} \mathbf{h}_{ij}\| = g_{ij} \kappa_i, \quad j \neq i, \quad (5)$$

$$\tilde{\beta}_i \triangleq \|\mathbf{\Pi}_{\mathbf{h}_{ii}}^\perp \mathbf{h}_{ij}\| = \sqrt{g_{ij}^2 - \beta_i^2} = g_{ij} \sqrt{1 - \kappa_i^2}, \quad j \neq i. \quad (6)$$

III. ACHIEVABLE RATE REGION OF SIC CAPABLE RXS

In this section, we give, for completeness, the definition of the achievable rate region for the described scenario [12], [13].

We also denote the core optimization problem that we need to solve to find a point on the Pareto boundary.

Each pair of beamforming vectors ($\mathbf{w}_1, \mathbf{w}_2$) and combination of decoding strategies (decode the interference (d) or treat it as noise (n)) is associated with a pair of maximum achievable rates. We denote by $R_i^{xy}(\mathbf{w}_1, \mathbf{w}_2)$ the rate of link $i = 1, 2$, in bits per channel use (bpcu), where x and y are the decoding strategies (n or d) of RX $_1$ and RX $_2$, respectively. For each pair of decoding strategies, we obtain a rate region by taking the union over all libe beamforming vectors, i.e.,

$$\mathcal{R}^{xy} \triangleq \bigcup_{(\mathbf{w}_1, \mathbf{w}_2) \in \mathcal{W}^2} (R_1^{xy}(\mathbf{w}_1, \mathbf{w}_2), R_2^{xy}(\mathbf{w}_1, \mathbf{w}_2)). \quad (7)$$

The achievable rate region: The rate region for the MISO IC with SIC capability is obtained as the union of the regions corresponding to all decoding scenarios, i.e., $\mathcal{R} = \mathcal{R}^{nn} \cup \mathcal{R}^{dn} \cup \mathcal{R}^{nd} \cup \mathcal{R}^{dd}$. Next, for each decoding scenario and a given pair of beamforming vectors ($\mathbf{w}_1, \mathbf{w}_2$), we give the maximum achievable rates [12], [13].

\mathcal{R}^{nn} - Both RXs treat the interference as noise: When both RXs treat the interference as noise, the maximum achievable rates of the links are [22]

$$R_1^{nn}(\mathbf{w}_1, \mathbf{w}_2) = \log_2 \left(1 + \frac{p_1(\mathbf{w}_1)}{q_1(\mathbf{w}_2) + \sigma_1^2} \right) \quad \text{and} \quad (8)$$

$$R_2^{nn}(\mathbf{w}_1, \mathbf{w}_2) = \log_2 \left(1 + \frac{p_2(\mathbf{w}_2)}{q_2(\mathbf{w}_1) + \sigma_2^2} \right).$$

\mathcal{R}^{dn} - RX $_1$ decodes the interference, RX $_2$ treats it as additive noise: Since RX $_1$ decodes and subtracts the interference caused by TX $_2$, it experiences an interference-free signal and the maximum achievable rate for link 1 is

$$R_1^{dn}(\mathbf{w}_1) = \log_2 (1 + p_1(\mathbf{w}_1) / \sigma_1^2). \quad (9)$$

RX $_1$ is able to decode the interference from TX $_2$, considering its own signal as noise, if the rate of link 2 is upper bounded by $\log_2 (1 + q_1(\mathbf{w}_2) / (p_1(\mathbf{w}_1) + \sigma_1^2))$. Since RX $_2$ does not decode the interference, the rate of link 2 is also upper bounded by $\log_2 (1 + p_2(\mathbf{w}_2) / (q_2(\mathbf{w}_1) + \sigma_2^2))$. Hence the maximum achievable rate for link 2 is given by

$$R_2^{dn}(\mathbf{w}_1, \mathbf{w}_2) = \log_2 \left(1 + \min \left\{ \frac{q_1(\mathbf{w}_2)}{p_1(\mathbf{w}_1) + \sigma_1^2}, \frac{p_2(\mathbf{w}_2)}{q_2(\mathbf{w}_1) + \sigma_2^2} \right\} \right), \quad (10)$$

where we have used the fact that the logarithm is a monotonously increasing function.

For link 2, we note that the rate is not necessarily selected to fully utilize the signal-to-interference-plus-noise (SINR) ratio at RX $_2$. Actually, link 2 might hold back on its rate to enable RX $_1$ to decode the interfering signal.²

\mathcal{R}^{nd} - RX $_2$ decodes the interference, RX $_1$ treats it as additive noise: This case is identical to \mathcal{R}^{dn} , but with interchanged indices.

\mathcal{R}^{dd} - Both RXs decode the interference: Both RXs decode the interference before decoding their desired signals. Since RX $_1$ decodes the interference from TX $_2$, the rate of

²This fact was not exploited in [22, Prop. 6 a)], so the description there led to an over-restrictive condition, hence, to a smaller achievable rate region.

link 1 is upper bounded by $\log_2(1 + p_1(\mathbf{w}_1)/\sigma_1^2)$. RX_2 can decode the interference caused by TX_1 if the rate of link 1 is upper bounded by $\log_2(1 + q_2(\mathbf{w}_1)/(p_2(\mathbf{w}_2) + \sigma_2^2))$. Then, the maximum achievable rate for link 1 is

$$R_1^{dd}(\mathbf{w}_1, \mathbf{w}_2) = \log_2 \left(1 + \min \left\{ \frac{p_1(\mathbf{w}_1)}{\sigma_1^2}, \frac{q_2(\mathbf{w}_1)}{p_2(\mathbf{w}_2) + \sigma_2^2} \right\} \right). \quad (11)$$

By symmetry, the maximum achievable rate of link 2 is

$$R_2^{dd}(\mathbf{w}_1, \mathbf{w}_2) = \log_2 \left(1 + \min \left\{ \frac{p_2(\mathbf{w}_2)}{\sigma_2^2}, \frac{q_1(\mathbf{w}_2)}{p_1(\mathbf{w}_1) + \sigma_1^2} \right\} \right). \quad (12)$$

The problem of interest is to find the so-called Pareto boundary of the region \mathcal{R} , which consists of PO rate pairs.

Definition 1. A point $(R_1^*, R_2^*) \in \mathcal{R}$ is (weakly) Pareto-optimal if there is no other point $(R_1, R_2) \in \mathcal{R}$ with $R_1 > R_1^*$ and $R_2 > R_2^*$.

Graphically, the Pareto boundary is the north-east boundary of the region and due to Def. 1 it also includes the horizontal and vertical segments. In order to find the Pareto boundary of \mathcal{R} , we first find the Pareto boundaries of \mathcal{R}^{nn} , \mathcal{R}^{dn} , \mathcal{R}^{nd} , and \mathcal{R}^{dd} . Second, we consider as boundary of \mathcal{R} the boundary of the union of the four \mathcal{R}^{xy} regions. We denote by \mathcal{B}^{xy} the boundary of \mathcal{R}^{xy} and by \mathcal{B} the boundary of \mathcal{R} . In [25, Lem. 1.2], it is proven that \mathcal{R}^{nn} is compact and normal under the assumptions in Sec. II. It is straightforward to extend this proof to include \mathcal{R}^{nd} , \mathcal{R}^{dn} , and \mathcal{R}^{dd} as well. Therefore, we conclude that the Pareto boundaries \mathcal{B}^{nn} , \mathcal{B}^{dn} , \mathcal{B}^{nd} , and \mathcal{B}^{dd} are closed.

We can find a point (R_1^*, R_2^*) on \mathcal{B}^{xy} when the rate of one communication link, e.g., R_1^* , is given [26, Prop. 6.2]. The other rate, R_2^* , is the maximum one we simultaneously achieve, e.g., see the dashed lines in Fig. 3 for \mathcal{R}^{nn} , and we find it by the following rate optimization problem³

$$\text{maximize}_{(\mathbf{w}_1, \mathbf{w}_2) \in \mathcal{W}^2} R_2^{xy}(\mathbf{w}_1, \mathbf{w}_2) \quad (13)$$

$$\text{subject to } R_1^{xy}(\mathbf{w}_1, \mathbf{w}_2) = R_1^*. \quad (14)$$

The optimization (13)–(14) accepts as input the coordinate R_1^* of the sought PO rate pair and yields as optimal value the other coordinate R_2^* and as optimal solution the enabling PO pair of beamforming vectors $(\mathbf{w}_1^*, \mathbf{w}_2^*)$. The choice of using R_1^* as input to the optimization is arbitrary. By the symmetry of the problem, we can choose R_2^* as input and have R_1^* as the optimal value. In the next sections, we derive efficient methods for solving (13)–(14) for all SIC-constituent regions. Since the logarithm is monotonic, we use the equivalent reformulation of (13)–(14) as an SINR optimization, where the input parameter is γ_1^* , i.e., the SINR (or the SNR after interference cancellation) required to achieve R_1^* .

IV. BOTH RXS TREAT THE INTERFERENCE AS NOISE

In this section, we compute the boundary \mathcal{B}^{nn} . We let \bar{R}_1^{nn} denote the maximum rate of link 1, achieved when TX_1 operates “selfishly” by using its maximum-ratio (MR) transmit beamforming vector $\mathbf{w}_1^{\text{MR}} = \arg \max_{\mathbf{w}_1 \in \mathcal{W}} p_1(\mathbf{w}_1) =$

$\mathbf{h}_{11}/\|\mathbf{h}_{11}\|$ and TX_2 operates “altruistically” by using its zero-forcing (ZF) transmit beamforming vector $\mathbf{w}_2^{\text{ZF}} = \arg \max_{\mathbf{w}_2 \in \mathcal{W}} p_2(\mathbf{w}_2) = \mathbf{\Pi}_{\mathbf{h}_{21}}^\perp \mathbf{h}_{22} / \|\mathbf{\Pi}_{\mathbf{h}_{21}}^\perp \mathbf{h}_{22}\|$ [22].

This combination of transmit strategies yields the PO point $(\bar{R}_1^{nn}, \underline{R}_2^{nn}) \triangleq (R_1^{nn}(\mathbf{w}_1^{\text{MR}}, \mathbf{w}_2^{\text{ZF}}), R_2^{nn}(\mathbf{w}_1^{\text{MR}}, \mathbf{w}_2^{\text{ZF}}))$ where

$$\bar{R}_1^{nn} = \log_2 \left(1 + \frac{\|\mathbf{h}_{11}\|^2}{\sigma_1^2} \right) = \log_2 \left(1 + \frac{g_{11}^2}{\sigma_1^2} \right) \quad \text{and} \quad (15)$$

$$\underline{R}_2^{nn} = \log_2 \left(1 + \frac{\|\mathbf{\Pi}_{\mathbf{h}_{21}}^\perp \mathbf{h}_{22}\|^2}{\|\mathbf{\Pi}_{\mathbf{h}_{11}} \mathbf{h}_{12}\|^2 + \sigma_2^2} \right) = \log_2 \left(1 + \frac{\alpha_2^2}{\beta_1^2 + \sigma_2^2} \right). \quad (16)$$

The rate in (16) is the lowest strongly PO rate of link 2 [22]. Interchanging the indices in (15)–(16) we get the point $(\underline{R}_1^{nn}, \bar{R}_2^{nn})$. As illustrated by the example in Fig. 3, these points split \mathcal{B}^{nn} into three segments. The weakly PO horizontal (vertical) segment $[(0, \bar{R}_2^{nn}), (\underline{R}_1^{nn}, \bar{R}_2^{nn})]$ ($[(\bar{R}_1^{nn}, 0), (\bar{R}_1^{nn}, \underline{R}_2^{nn})]$) is achieved when TX_1 (TX_2) uses the MR beamforming vector and TX_2 (TX_1) uses the ZF beamforming vector, adapting the transmit power in $[0, 1]$.

The remainder of this section focuses on the strongly PO segment between $(\underline{R}_1^{nn}, \bar{R}_2^{nn})$ and $(\bar{R}_1^{nn}, \underline{R}_2^{nn})$. Inserting (8) into (13)–(14) and equivalently reformulating the rate maximization to SINR maximization, we obtain

$$\text{maximize}_{(\mathbf{w}_1, \mathbf{w}_2) \in \mathcal{W}^2} \frac{p_2(\mathbf{w}_2)}{q_2(\mathbf{w}_1) + \sigma_2^2} \quad (17)$$

$$\text{subject to } \frac{p_1(\mathbf{w}_1)}{q_1(\mathbf{w}_2) + \sigma_1^2} = \gamma_1^*. \quad (18)$$

From (15), we see that constraint (18), hence the optimization, is feasible when $\gamma_1^* \leq g_{11}^2/\sigma_1^2$. The formulation (17)–(18) is non-convex since the objective function (17) and the equality constraint (18) consist of fractions of quadratics.

In Secs. IV-A and IV-B, we propose two methods to find very efficiently the global optimal solution. The main difference between these methods is the input required to yield the entire boundary; in the first method it is different choices for one of the PO SINR values, whereas in the second method it is different choices for one of the PO beamforming vectors. Both methods have computational complexity that is constant in the number of transmit antennas. The method in Sec. IV-A can be interpreted as solving an underlay cognitive radio problem where the secondary user, here link 2, maximizes its rate under various quality-of-service constraints for the primary user, here link 1. Also, this method can be used to determine if a rate point (R_1, R_2) is feasible. Let $R_1^* = R_1$ be the input to (17)–(18). Then, if $R_2^* \geq R_2$, we can conclude that (R_1, R_2) is feasible. The interpretation of the method in Sec. IV-B is that TX_1 fixes its beamforming strategy and TX_2 seeks the best-response strategy to end up at a PO point.

A. Numerical Method

The numerical method proposed in this section is a two-fold improvement of the one we presented in [23]. First, we exploit the parameterization [13] of the PO beamforming

³Note that the optimization is only over the set of beamforming vectors satisfying the power constraints included in the set \mathcal{W}^2 .

vectors to reduce, without loss of optimality, the feasible set from \mathcal{W}^2 , i.e., a bounded convex set in \mathbb{R}^{4n_T} , to the bounded positive quadrant. Second, we equivalently reformulate the optimization problem to further reduce the feasible set to a line segment in \mathbb{R} . The resulting problem is a scalar quasi-concave problem that needs to be solved once to yield a PO point, whereas the parameterized convex formulation in [23] required several iterations of the bisection method.

From [13, Corollary 1], we know that the PO beamforming vectors of the \mathcal{R}^{nn} region can be parameterized as

$$\mathbf{w}_i(x_i) = x_i \frac{\mathbf{\Pi}_{\mathbf{h}_{ij}} \mathbf{h}_{ii}}{\|\mathbf{\Pi}_{\mathbf{h}_{ij}} \mathbf{h}_{ii}\|} + \sqrt{1-x_i^2} \frac{\mathbf{\Pi}_{\mathbf{h}_{ij}}^\perp \mathbf{h}_{ii}}{\|\mathbf{\Pi}_{\mathbf{h}_{ij}}^\perp \mathbf{h}_{ii}\|}, \quad (19)$$

where $0 \leq x_i \leq 1$ for $i, j = 1, 2$ and $j \neq i$. Note that (19) consists of a single nonnegative real parameter per beamforming vector. Inserting (19) into (2), we get

$$\begin{aligned} p_i(\mathbf{w}_i) &= \left(x_i \|\mathbf{\Pi}_{\mathbf{h}_{ij}} \mathbf{h}_{ii}\| + \sqrt{1-x_i^2} \|\mathbf{\Pi}_{\mathbf{h}_{ij}}^\perp \mathbf{h}_{ii}\| \right)^2 \\ &= \left(\alpha_i x_i + \tilde{\alpha}_i \sqrt{1-x_i^2} \right)^2, \end{aligned} \quad (20)$$

$$q_j(\mathbf{w}_i) = x_i^2 \frac{|\mathbf{h}_{ij}^H \mathbf{h}_{ii}|^2}{\|\mathbf{\Pi}_{\mathbf{h}_{ij}} \mathbf{h}_{ii}\|^2} = g_{ij}^2 x_i^2. \quad (21)$$

From [19], we know that, for PO points, $x_i \leq \alpha_i/g_{ii} = \kappa_i$. This value maximizes (20) and corresponds to the MR transmit beamforming vector. Further increase of x_i will just increase the interference and decrease the desired signal power.

Inserting (20) and (21) into (17)–(18) and performing straightforward algebraic manipulations, including taking the square root, we get the equivalent reformulation

$$\underset{0 \leq x_1, x_2 \leq 1}{\text{maximize}} \quad \frac{\alpha_2 x_2 + \tilde{\alpha}_2 \sqrt{1-x_2^2}}{\sqrt{g_{12}^2 x_1^2 + \sigma_2^2}} \quad (22)$$

$$\text{subject to} \quad \frac{\alpha_1 x_1 + \tilde{\alpha}_1 \sqrt{1-x_1^2}}{\sqrt{g_{21}^2 x_2^2 + \sigma_1^2}} = \sqrt{\gamma_1^*}, \quad (23)$$

where the constants $\alpha_1, \tilde{\alpha}_1, \alpha_2, \tilde{\alpha}_2, g_{12}, g_{21}$ are all positive, as defined in Sec. II. We further simplify the notation defining

$$u_i(x_i) \triangleq \alpha_i x_i + \tilde{\alpha}_i \sqrt{1-x_i^2} \quad i = 1, 2 \quad \text{and} \quad (24)$$

$$v_i(x_j) \triangleq \sqrt{g_{ji}^2 x_j^2 + \sigma_i^2} \quad i, j = 1, 2, \quad j \neq i. \quad (25)$$

It is straightforward to verify that $u_i(x_i)$ is concave and non-decreasing for $x_i \leq \kappa_i$. Moreover, since $v_i(x_j)$ is a norm, it is a convex and non-decreasing function in x_j . Then, we make the following observation:

Lemma 1. *The objective function (22) and the left-hand-side (LHS) of the constraint (23) are quasi-concave functions.*

Proof: Note that $u_i(x_i)/v_i(x_j) \geq c$ is equivalent to $cv_i(x_j) - u_i(x_i) \leq 0$ since $v_i(x_i) > 0$. Since $cv_i(x_j)$ is convex for all $c \geq 0$ and $u_i(x_i)$ is concave, $cv_i(x_j) - u_i(x_i) \leq 0$ defines a convex set. Hence, we conclude that the objective (22) and the LHS of constraint (23) are quasi-concave functions [27, Ch. 3]. ■

Due to the equality in (23), the problem (22)–(23) is not

quasi-concave as it stands [28], but in the following we equivalently reformulate it into a quasi-concave problem in one scalar variable. We solve equation (23) for x_2 , keeping the positive root, as

$$x_2 = \sqrt{\frac{u_1^2(x_1) - \gamma_1^* \sigma_1^2}{g_{21}^2 \gamma_1^*}} \triangleq w(x_1). \quad (26)$$

Since a function of the form $\sqrt{t^2 - a}$ is concave and non-decreasing for $t \geq \sqrt{a}$, $a \geq 0$ and $u_1(x_1)$ is concave and non-decreasing for $x_1 \leq \kappa_1$, we conclude that $w(x_1)$ is a concave and non-decreasing function of $x_1 \leq \kappa_1$ [27, Ch. 3.2].

The constraints $0 \leq x_2 \leq \kappa_2$ introduce lower and upper bounds on x_1 . Since $x_2 \geq 0$, it follows from (26) that $u_1(x_1) \geq \sqrt{\gamma_1^* \sigma_1^2}$. Then, from (24) and $x_1 \geq 0$, it follows that we must have $x_1 \geq \underline{x}_1$, where

$$\underline{x}_1 \triangleq \max \left\{ 0, \kappa_1 \sqrt{\frac{\gamma_1^*}{\bar{\gamma}_1^{nn}}} - \sqrt{1 - \kappa_1^2} \sqrt{1 - \frac{\gamma_1^*}{\bar{\gamma}_1^{nn}}} \right\}. \quad (27)$$

Note that \underline{x}_1 is real for $\gamma_1^* \leq \bar{\gamma}_1^{nn} \triangleq 2\bar{R}_1^{nn} - 1 = g_{11}^2/\sigma_1^2$. Furthermore, for the upper limits we must have $x_2 = w(x_1) \leq \kappa_2$ and $x_1 \leq \kappa_1$, which imply $x_1 \leq \bar{x}_1$, where

$$\bar{x}_1 \triangleq \begin{cases} \kappa_1 \sqrt{\frac{\gamma_1^*}{\gamma_1^{\text{MR}}}} - \sqrt{1 - \kappa_1^2} \sqrt{1 - \frac{\gamma_1^*}{\gamma_1^{\text{MR}}}}, & \gamma_1^* \leq \gamma_1^{\text{MR}}, \\ \kappa_1, & \gamma_1^* > \gamma_1^{\text{MR}}, \end{cases} \quad (28)$$

and where $\gamma_1^{\text{MR}} \triangleq g_{11}^2/(g_{21}^2 \kappa_1^2 + \sigma_1^2)$ is the SINR of link 1 when both TXs use the MR beamforming vectors, which yield the so-called Nash Equilibrium [22]. Note that $\gamma_1^{\text{MR}} < \bar{\gamma}_1^{nn}$, where the latter is the SNR of RX₁ at the single-user point of the rate region. It can be verified that $\bar{x}_1 \geq 0$ since $\gamma_1^* \geq \underline{\gamma}_1^{nn} \triangleq 2\underline{R}_1^{nn} - 1$.

Inserting (26) in (22), along with the lower and upper bounds (27) and (28), respectively, yields the scalar optimization problem

$$\underset{\underline{x}_1 \leq x_1 \leq \bar{x}_1}{\text{maximize}} \quad \frac{u_2(w(x_1))}{v_2(x_1)} \triangleq s(x_1). \quad (29)$$

Note that the objective function corresponds to the square root of the SINR of link 2, i.e., $s(x_1) = \sqrt{\gamma_2}$. Next, we study its properties and prove that it is quasi-concave.

Lemma 2. *The function $s(x_1)$ is quasi-concave for $\underline{x}_1 < x_1 < \bar{x}_1$.*

Proof: First, we observe that $s(x_1)$ is at least twice continuously differentiable for $\underline{x}_1 < x < \bar{x}_1$. Second, we show that $s'(x_1) = 0$ implies that $s''(x_1) < 0$ and it follows that $s(x_1)$ is quasi-concave [27, Ch. 3.4.3].

The first derivative of $s(x_1)$ is

$$s'(x_1) = \frac{w'(x_1)u_2'(w(x_1))v_2(x_1) - u_2(w(x_1))v_2'(x_1)}{v_2^2(x_1)} \quad (30)$$

and the second derivative is

$$\begin{aligned} s''(x_1) &= \frac{1}{v_2^2(x_1)} \left(w''(x_1)u_2'(w(x_1))v_2(x_1) + \right. \\ &\quad \left. + (w'(x_1))^2 u_2''(w(x_1))v_2(x_1) - u_2(w(x_1))v_2''(x_1) \right). \end{aligned} \quad (31)$$

We know that $w(x_1)$ is concave and non-decreasing for $x_1 \leq \kappa_1$, $v_2(x_1)$ is convex and non-decreasing and $u_2(x_2)$ is concave.⁴ Therefore, we conclude that the second and third terms of (31) are non-positive. Also, we note that the second term is zero only if $x_1 = \kappa_1$ and the third term is zero only if $x_1 = 0$. Hence, we conclude that the sum of the second and third terms in (31) is always negative. It remains to show that the first term in (31) is non-positive for a stationary point x_1^* . We know that $w''(x_1^*) \leq 0$ and $v_2(x_1^*) > 0$, so we must show that $u_2'(w(x_1^*)) \geq 0$. For a stationary point, the first derivative is zero, so from (30) it follows that

$$u_2'(w(x_1^*)) = \frac{u_2(w(x_1^*))v_2'(x_1^*)}{w'(x_1^*)v_2(x_1^*)} \geq 0 \quad (32)$$

since $u_2(w(x_1))$, $v_2'(x_1)$, $w'(x_1)$, and $v_2(x_1)$ all are non-negative for $x_1 \leq \kappa_1$. Since $s'(x_1) = 0$ implies $s''(x_1) < 0$, we conclude that $s(x_1)$ is quasi-concave, [27, Ch. 3.4.3] ■

Since problem (29) has a single real variable and the objective function is quasi-concave, the optimum solution can be found very efficiently. Since the objective function is monotonously increasing (decreasing) to the left (right) of the stationary point, a gradient method can be used. In Tab. I, we propose a method that computes strongly PO points of \mathcal{R}^{nn} . As input, the method requires the channel constants, the noise variances, and the number M of requested boundary points. The output is stored in the vectors $\mathbf{r}_1, \mathbf{r}_2 \in \mathbb{R}^M$. The rates in \mathbf{r}_1 are obtained by uniform sampling over the interval $[\underline{R}_1^{nn}, \overline{R}_1^{nn}]$. In line 4, we compute the end point $(\underline{R}_2^{nn}, \overline{R}_2^{nn})$. For each boundary point, we compute the lower and upper bounds \underline{x}_1 and \overline{x}_1 , respectively, and ensure that the solution lies in the interval $[\underline{x}_1, \overline{x}_1]$. In line 8, the x_1^* corresponding to the previously computed point is used as initial value for the next point on the boundary. The reason is that we expect that the solution will not change significantly for two nearby points. In lines 10–14, we find the optimal solution x_1^* by a gradient ascend method. In each repetition, we compute the derivative $s'(x_1)$ and then find a step length t , by backtracking line search [27, Ch. 9.2]. This is repeated until the improvement from the previous iteration is smaller than some predefined tolerance ϵ . Since $s(x_1)$ is quasi-concave, its derivative can be small without being close to the optimum. Hence, ϵ has to be chosen very small. In line 20, the end point $(\underline{R}_1^{nn}, \underline{R}_2^{nn})$ is computed.

B. Closed-Form Parameterization

In this section, we use the Karush-Kuhn-Tucker (KKT) conditions of the optimization problem (22)–(23) in order to derive a closed-form relation between the parameters of the beamforming vectors that jointly yield a PO rate point. A preliminary version of this method was presented in [1]; herein, we elaborate the derivations and provide a proof of global optimality. The latter is achieved using the parameterization (19), whereas a different parameterization was used in [1].

In general, the KKT conditions only provide necessary conditions for global optimality. However, we show that for

⁴We could have used the fact the $u_2(w(x_1))$ is also non-decreasing for $x_1 \leq \overline{x}_1$, to obtain a simpler proof. However, in Sec VI, we need this more general case.

1:	Input: $g_{ij}, \kappa_i, \sigma_i^2, i, j = 1, 2, M$, and ϵ
2:	Output: \mathcal{B}^{nn} given by vectors $\mathbf{r}_1, \mathbf{r}_2 \in \mathbb{R}^M$
3:	$\mathbf{r}_1 = [\underline{R}_1^{nn} : (\overline{R}_1^{nn} - \underline{R}_1^{nn}) / (M - 1) : \overline{R}_1^{nn}]$
4:	$\mathbf{r}_2(1) = \overline{R}_2^{nn}, x_1^* = 0$
5:	for $k = 2 : M - 1$
6:	$\gamma_1^* = 2^{r_1(k)} - 1$
7:	Compute \underline{x}_1 and \overline{x}_1 using (27) and (28)
8:	$x_1^{(0)} = [x_1^*]_{\underline{x}_1}^{\overline{x}_1}$
9:	$l = 0$
10:	repeat
11:	Compute $s'(x_1^{(l)})$ and determine step size t
12:	$x_1^{(l+1)} = [x_1^{(l)} + ts'(x_1^{(l)})]_{\underline{x}_1}^{\overline{x}_1}$
13:	$l \leftarrow l + 1$
14:	until $ s(x_1^{(l)}) - s(x_1^{(l-1)}) < \epsilon$
15:	$x_1^* = x_1^{(l)}$
16:	Compute $x_2^* = w(x_1^*)$ using (26)
17:	Compute $\mathbf{w}_i^* = \mathbf{w}_i(x_i^*)$ using (19)
18:	Compute $\mathbf{r}_2(k) = \mathbf{R}_2^* = \mathbf{R}_2^{nn}(\mathbf{w}_1^*, \mathbf{w}_2^*)$ using (8)
19:	end
20:	$\mathbf{r}_2(M) = \underline{R}_2^{nn}, x_1^* = \kappa_1, x_2^* = 0$

TABLE I
NUMERICAL METHOD TO COMPUTE \mathcal{B}^{nn}

this specific problem, the KKT conditions are also sufficient. Towards this direction, we relax the equality constraint (23) to a lower-bound inequality.⁵ Then, due to Lem. 1, the relaxed optimization problem (22)–(23) falls into the class of quasi-concave problems [28]. Th. 1 in [28] gives a number of sufficient conditions for global optimality of the solution to the KKT conditions of a constrained quasi-concave program. It suffices that one of these conditions is satisfied. Condition a) is that the gradient of the objective function should have at least one negative component for a solution that satisfies the KKT conditions. By simple inspection of the objective function (22), it follows that:

Lemma 3. *The objective (22) is decreasing with $x_1 \geq 0$, for fixed x_2 .*

Hence, due to Lem. 3, the relaxed version of the problem (22)–(23) satisfies condition a) of Th. 1 in [28]. Then, from Lem. 1, Lem. 3, and [28, Th. 1], we have the following result:

Proposition 1. *The KKT conditions of the relaxed problem (22)–(23) are sufficient conditions for global optimality.*

For notational convenience, we make the bounding constraints on x_i implicit, i.e., we declare a solution of the KKT conditions feasible only if it adheres to the bounding

⁵By contradiction, we can show that this relaxation is tight at the optimum. Assume that the optimal solution meets (23) by strict inequality. Then there is room to increase x_2 or decrease x_1 in order to make the objective (22) larger. This is illustrated by the dashed lines in Fig. 3. Hence the relaxed problem is equivalent to the original one.

constraints. The Lagrange function of the relaxed (22)–(23) is

$$\mathcal{L}(x_1, x_2, \mu) = \frac{u_2(x_2)}{v_2(x_1)} + \mu \left(\frac{u_1(x_1)}{v_1(x_2)} - \sqrt{\gamma_1^*} \right), \quad (33)$$

where the Lagrange multiplier μ is non-negative. Hence, the KKT conditions are [27]

$$\mu \left(\frac{u_1(x_1)}{v_1(x_2)} - \sqrt{\gamma_1^*} \right) = 0, \quad (34)$$

$$\frac{\partial \mathcal{L}}{\partial x_1} = -\frac{v_2'(x_1)u_2(x_2)}{v_2^2(x_1)} + \mu \frac{u_1'(x_1)}{v_1(x_2)} = 0, \quad (35)$$

$$\frac{\partial \mathcal{L}}{\partial x_2} = \frac{u_2'(x_2)}{v_2(x_1)} - \mu \frac{v_1'(x_2)u_1(x_1)}{v_1^2(x_2)} = 0. \quad (36)$$

In (34)–(36), we avoided explicitly including the primal feasibility constraints, since (22)–(23) is always feasible if we choose $\gamma_1^* \leq g_{11}^2/\sigma_1^2$. Also, it is straightforward to verify that the corresponding Lagrange multipliers must be zero. We use the KKT conditions to find a relation between the parameters x_1 and x_2 that jointly yield PO points. Since we are not looking for a specific PO point, we can disregard condition (34). Once we have found a pair (x_1^*, x_2^*) that solves (35)–(36) for some μ^* , we insert the triplet (x_1^*, x_2^*, μ^*) into (34) to find γ_1^* . Clearly $(x_1^*, x_2^*, \gamma_1^*, \mu^*)$ solves the KKT conditions (34)–(36).

When $x_1 > 0$, we can verify from (35) that $\mu > 0$. Then, we use (35) and (36) to solve for μ . Equating the solutions, we get the relation

$$\frac{u_2'(x_2)v_1^2(x_2)}{v_1'(x_2)v_2(x_1)u_1(x_1)} = \frac{v_2'(x_1)v_1(x_2)u_2(x_2)}{u_1'(x_1)v_2^2(x_1)}. \quad (37)$$

By collecting all functions of x_1 and x_2 in the LHS and RHS, respectively, we equivalently rewrite (37) as

$$f(x_1) \triangleq \frac{u_1'(x_1)v_2^2(x_1)}{v_2'(x_1)v_2(x_1)u_1(x_1)} = \frac{v_1'(x_2)v_1(x_2)u_2(x_2)}{u_2'(x_2)v_1^2(x_2)} \triangleq g(x_2). \quad (38)$$

The LHS and RHS of (38) are functions of only x_1 and x_2 , respectively, which we denote as $f(x_1)$ and $g(x_2)$, respectively. In order to find a PO point, we fix x_1 at a specific value x_1^* and then solve $g(x_2) = f(x_1^*)$ to get x_2^* .

Due to the square roots, it is complicated to solve for x_2 as it stands. Instead, we use the alternative parameterization, that the PO beamforming vectors are linear combinations of the MR and ZF beamforming vectors [13, Corollary 2], i.e.,

$$\mathbf{w}_i^{\text{PO}}(\lambda_i) = \frac{\lambda_i \mathbf{w}_i^{\text{MR}} + (1 - \lambda_i) \mathbf{w}_i^{\text{ZF}}}{\|\lambda_i \mathbf{w}_i^{\text{MR}} + (1 - \lambda_i) \mathbf{w}_i^{\text{ZF}}\|}, \quad (39)$$

where $\lambda_i \in [0, 1]$. To go from the parameterization in (19) to that in (39), we use the mapping

$$\begin{aligned} x_i &= \phi_i(\lambda_i) \triangleq \frac{\kappa_i \lambda_i}{\|\lambda_i \mathbf{w}_i^{\text{MR}} + (1 - \lambda_i) \mathbf{w}_i^{\text{ZF}}\|} \\ &= \frac{\kappa_i \lambda_i}{\sqrt{2\rho_i \lambda_i^2 - 2\rho_i \lambda_i + 1}}, \end{aligned} \quad (40)$$

where $\rho_i \triangleq 1 - \sqrt{1 - \kappa_i^2}$. Since $0 < \kappa_i < 1$, we have

$$\frac{d\phi_i}{d\lambda_i} = \frac{\kappa_i(1 - \rho_i \lambda_i)}{(2\rho_i \lambda_i^2 - 2\rho_i \lambda_i + 1)^{3/2}} > 0. \quad (41)$$

Hence, it follows that (40) is a one-to-one mapping between x_i and λ_i and the problem of solving $g(x_2) = f(x_1^*)$ with respect to x_2 is equivalent to that of solving $g(\phi_2(\lambda_2)) = f(\phi_1(\lambda_1^*))$ with respect to λ_2 . By inserting (40) into (38), we equivalently write $g(\phi_2(\lambda_2)) = f(\phi_1(\lambda_1^*))$ as

$$\frac{\lambda_2(1 - \rho_2 \lambda_2)(\rho_2 \lambda_2 + (1 - \rho_2))}{(1 - \lambda_2)(\rho_2(2 - \rho_2 + 2\zeta_2)\lambda_2^2 - 2\rho_2 \zeta_2 \lambda_2 + \zeta_2)} = f(\phi_1(\lambda_1^*)), \quad (42)$$

where $\zeta_i \triangleq \sigma_j^2/g_{ij}^2$, $i, j = 1, 2$, $j \neq i$. In (42), we see that $g(\phi_2(\lambda_2))$ is a fraction of cubic polynomials. Since $f(\phi_1(\lambda_1^*))$ is a constant, we write (42) as the cubic equation

$$c_3 \lambda_2^3 + c_2 \lambda_2^2 + c_1 \lambda_2 + c_0 = 0. \quad (43)$$

The coefficients of the cubic equation (43) are

$$\begin{cases} c_0 \triangleq -\zeta_2 f(\lambda_1^*), \\ c_1 \triangleq (1 + 2\rho_2)\zeta_2 f(\lambda_1^*) + (1 - \rho_2), \\ c_2 \triangleq -\rho_2(2 - \rho_2 + 4\zeta_2)f(\phi_1(\lambda_1^*)) + \rho_2^2, \\ c_3 \triangleq \rho_2(2 - \rho_2 + 2\zeta_2)f(\phi_1(\lambda_1^*)) - \rho_2^2. \end{cases} \quad (44)$$

Cubic equations can be solved in closed form [29]. The roots of (43) are three candidates for λ_2^* .⁶ Since $\lambda_1^* \in [0, 1]$, we have the following three cases.

- $\lambda_1^* = 0$: From (16) and (39) we know that $\lambda_2^* = 1$.
- $0 < \lambda_1^* < 1$: We find the roots of (43) and keep the roots that satisfy the constraint $0 \leq \lambda_2 \leq 1$. We can potentially have more than one feasible root, but from Prop. 1, we know that all feasible roots yield a PO solution.⁷
- $\lambda_1^* = 1$: Again, from (16) and (39) we see that $\lambda_2^* = 0$.

The overall method to compute the entire \mathcal{B}^{nn} is summarized in Tab. II. By uniform sampling of λ_1^* over the interval $[0, 1]$, we will cover the entire interval $[\underline{R}^{nn}, \overline{R}^{nn}]$. Once we have found the coefficients in Sec. II, the complexity is constant in the number of antennas.

1:	Input and output: same as in Tab. I
2:	for $\lambda_1^* = [0 : 1/(M-1) : 1]$
3:	Compute $f(\phi_1(\lambda_1^*))$ according to (38) and (40)
4:	$\lambda_2^* =$ roots of cubic equation (43) that are in $[0, 1]$
5:	Compute the rate point(s) using (8), (19), and (40)
6:	end

TABLE II
CLOSED-FORM METHOD TO COMPUTE \mathcal{B}^{nn}

V. ONLY ONE RX DECODES THE INTERFERENCE

In this section, we compute \mathcal{B}^{dn} on closed form. A condensed description of this method was given in [2].

Inserting the rate expressions (9) and (10) in the optimization problem (13)–(14) and equivalently reformulating the rate maximization to SINR maximization, we obtain

$$\underset{(\mathbf{w}_1, \mathbf{w}_2) \in \mathcal{W}^2}{\text{maximize}} \quad \min \left\{ \frac{q_1(\mathbf{w}_2)}{p_1(\mathbf{w}_1) + \sigma_1^2}, \frac{p_2(\mathbf{w}_2)}{q_2(\mathbf{w}_1) + \sigma_2^2} \right\} \quad (45)$$

$$\text{subject to} \quad p_1(\mathbf{w}_1)/\sigma_1^2 = \gamma_1^*. \quad (46)$$

⁶Note that any other choice of λ_1^* gives us a point in the interior of \mathcal{R}^{nn} .
⁷In [19] and [20], it was not made clear whether all feasible solutions to the corresponding cubic equation are optimal or not. Especially, equation (25) in [19] provides only necessary conditions for Pareto optimality [26, Ch. 6].

As with (17)–(18), we see that (45)–(46) is feasible when $\gamma_1^* \leq g_{11}^2/\sigma_1^2$. The formulation (45)–(46) is nonconvex, because the objective (45) is the minimum of two fractions of quadratic functions and (46) is a quadratic equality constraint.

In [12], it was shown that the PO beamforming vectors of the \mathcal{R}^{dn} region can be parameterized as

$$\mathbf{w}_1(x_1, y_1) = x_1 \frac{\mathbf{\Pi}_{\mathbf{h}_{12}} \mathbf{h}_{11}}{\|\mathbf{\Pi}_{\mathbf{h}_{12}} \mathbf{h}_{11}\|} + y_1 \frac{\mathbf{\Pi}_{\mathbf{h}_{12}}^\perp \mathbf{h}_{11}}{\|\mathbf{\Pi}_{\mathbf{h}_{12}}^\perp \mathbf{h}_{11}\|}, \quad (47)$$

$$\mathbf{w}_2(x_2) = x_2 \frac{\mathbf{\Pi}_{\mathbf{h}_{22}} \mathbf{h}_{21}}{\|\mathbf{\Pi}_{\mathbf{h}_{22}} \mathbf{h}_{21}\|} + \sqrt{1-x_2^2} \frac{\mathbf{\Pi}_{\mathbf{h}_{22}}^\perp \mathbf{h}_{21}}{\|\mathbf{\Pi}_{\mathbf{h}_{22}}^\perp \mathbf{h}_{21}\|}, \quad (48)$$

where $(x_1, y_1) \in \mathcal{Q} \triangleq \{(x, y) | x, y \geq 0, x^2 + y^2 \leq 1\}$ and $x_2 \in [0, 1]$. Note that this parameterization is different from (19) and (39) of \mathcal{R}^{nn} . An interpretation stemming from (47)–(48) is that on the Pareto boundary TX₂ uses full power, whereas TX₁ may not. Inserting (47)–(48) into (2), we get

$$p_1(\mathbf{w}_1) = \left(x_1 \|\mathbf{\Pi}_{\mathbf{h}_{12}} \mathbf{h}_{11}\| + y_1 \|\mathbf{\Pi}_{\mathbf{h}_{12}}^\perp \mathbf{h}_{11}\| \right)^2 = (\alpha_1 x_1 + \tilde{\alpha}_1 y_1)^2, \quad (49)$$

$$q_2(\mathbf{w}_1) = x_1^2 \frac{|\mathbf{h}_{12}^H \mathbf{h}_{11}|^2}{\|\mathbf{\Pi}_{\mathbf{h}_{12}} \mathbf{h}_{11}\|^2} = g_{12}^2 x_1^2, \quad (50)$$

$$p_2(\mathbf{w}_2) = x_2^2 \frac{|\mathbf{h}_{22}^H \mathbf{h}_{21}|^2}{\|\mathbf{\Pi}_{\mathbf{h}_{22}} \mathbf{h}_{21}\|^2} = g_{22}^2 x_2^2, \quad (51)$$

$$q_1(\mathbf{w}_2) = \left(x_2 \|\mathbf{\Pi}_{\mathbf{h}_{22}} \mathbf{h}_{21}\| + \sqrt{1-x_2^2} \|\mathbf{\Pi}_{\mathbf{h}_{22}}^\perp \mathbf{h}_{21}\| \right)^2 = \left(\beta_2 x_2 + \tilde{\beta}_2 \sqrt{1-x_2^2} \right)^2, \quad (52)$$

where the parameters $\alpha_1, \tilde{\alpha}_1, \beta_1, \tilde{\beta}_1, g_{12}, g_{22}$ are positive, as defined in Sec. II. When x_1 increases, both the power of the desired signal (49) and the interference (50) increase, whereas y_1 only increases the power of the desired signal. When x_2 increases, the desired signal power (51) increases.

Inserting (49)–(52) in (45)–(46), replacing the constraint (46) in the denominator of the first fraction of (45), and taking the square root, we equivalently obtain

$$\underset{\substack{(x_1, y_1) \in \mathcal{Q} \\ x_2 \in [0, 1]}}{\text{maximize}} \quad \min \left\{ \frac{\beta_2 x_2 + \tilde{\beta}_2 \sqrt{1-x_2^2}}{\sqrt{\sigma_1^2(\gamma_1^* + 1)}}, \frac{g_{22} x_2}{\sqrt{g_{12}^2 x_1^2 + \sigma_2^2}} \right\} \quad (53)$$

$$\text{subject to} \quad \alpha_1 x_1 + \tilde{\alpha}_1 y_1 = \sqrt{\gamma_1^* \sigma_1^2}. \quad (54)$$

By Lem. 1, we see that the two fractions in the objective function (53) are quasi-concave. Since the minimum of two quasi-concave functions is quasi-concave and (54) is linear, it follows that (53)–(54) is a quasi-concave problem.

We solve (53)–(54) in two steps. First we solve for (x_1, y_1) and then for x_2 . We note that x_1 appears only in the second fraction of (53) and in (54), whereas y_1 appears only in (54). The second fraction of (53) is monotonously decreasing with x_1 , for fixed x_2 , so we maximize it by minimizing x_1 , subject to the constraint (54), i.e.,

$$\underset{(x_1, y_1) \in \mathcal{Q}}{\text{minimize}} \quad x_1 \quad (55)$$

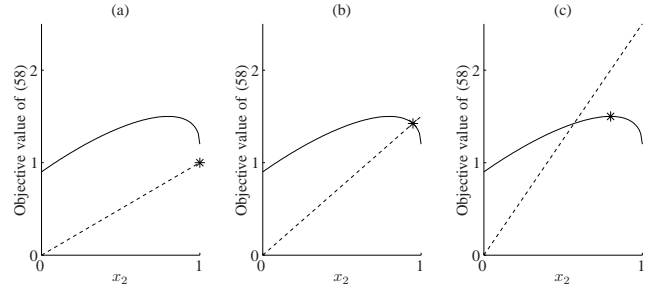


Fig. 1. Illustration of the three different cases in the proof of Prop. 2. The optimal solution is marked with a star. (a): $a = 1, b = 1.2, c = 0.9$; (b): $a = 1.5, b = 1.2, c = 0.9$; (c): $a = 2.5, b = 1.2, c = 0.9$.

$$\text{subject to} \quad y_1 = -\frac{\alpha_1}{\tilde{\alpha}_1} x_1 + \frac{\sqrt{\gamma_1^* \sigma_1^2}}{\tilde{\alpha}_1}. \quad (56)$$

The solution of this problem can be found by inspection, noting that the feasible set is the segment of the line (56) in \mathcal{Q} . When $\sqrt{\gamma_1^* \sigma_1^2}/\tilde{\alpha}_1 \leq 1$, this line segment does not intersect the unit-radius circle; hence, the optimum value is $x_1^* = 0$. The interpretation of this solution is that TX₁ uses the ZF beamforming vector, but contrary to the \mathcal{R}^{nn} case, it may not use full power in order to make interference cancellation possible. When $\sqrt{\gamma_1^* \sigma_1^2}/\tilde{\alpha}_1 > 1$, the line segment intersects the unit circle in two points; hence, the leftmost is the optimum. Inserting (56) into the quadratic equation of the unit circle, it is straightforward to determine that $x_1^* = \left(\alpha_1 \sqrt{\gamma_1^* \sigma_1^2} - \tilde{\alpha}_1 \sqrt{g_{11}^2 - \gamma_1^* \sigma_1^2} \right) / g_{11}^2$, where we have used the fact that $g_{11}^2 = \alpha_1^2 + \tilde{\alpha}_1^2$. The interpretation of this solution is that TX₁ uses full power in this case.

Given the optimal x_1^* , the optimal y_1^* is determined by (56), and the problem (53)–(54) only depends on x_2 , i.e.,

$$\underset{0 \leq x_2 \leq 1}{\text{maximize}} \quad \min \left\{ \frac{\beta_2 x_2 + \tilde{\beta}_2 \sqrt{1-x_2^2}}{\sqrt{(\gamma_1^* + 1)\sigma_1^2}}, \frac{g_{22} x_2}{\sqrt{g_{12}^2 (x_1^*)^2 + \sigma_2^2}} \right\}. \quad (57)$$

In order to simplify the notation, we define the constants $a \triangleq g_{22}/\sqrt{(x_1^*)^2 g_{12}^2 + \sigma_2^2}$, $b \triangleq \beta_2/\sqrt{\sigma_1^2(\gamma_1^* + 1)}$, and $c \triangleq \tilde{\beta}_2/\sqrt{\sigma_1^2(\gamma_1^* + 1)}$. Using these constants, we write (57) as

$$\underset{0 \leq x_2 \leq 1}{\text{maximize}} \quad \min \left\{ b x_2 + c \sqrt{1-x_2^2}, a x_2 \right\}. \quad (58)$$

Depending on the values of a, b , and c , we get three different cases for the objective functions in (58), as depicted in Fig. 1. In Fig. 1 (a), we have $a \leq b$ and it is clear that the optimum is at $x_2^* = 1$. The interpretation is that TX₂ uses the MR beamforming vector. The difference between the cases in Fig. 1 (b) and Fig. 1 (c) is whether the intersection of the curve with the straight line is to the left or right of the maximum of the curve. The curve $b x_2 + c \sqrt{1-x_2^2}$ is maximized for $x_2 = b/\sqrt{b^2 + c^2}$. The intersection of $b x_2 + c \sqrt{1-x_2^2}$ with $a x_2$ happens for $x_2 = c/\sqrt{c^2 + (a-b)^2}$. In Fig. 1 (b), the intersection is to the right of curve's maximum; hence,

$$\frac{c}{\sqrt{c^2 + (a-b)^2}} \geq \frac{b}{\sqrt{b^2 + c^2}} \Leftrightarrow ab \leq b^2 + c^2. \quad (59)$$

From Fig. 1 (b), we see that the optimum is at the intersection.

Hence, we have $x_2^* = c/\sqrt{c^2 + (a-b)^2}$. For the case in Fig. 1 (c), we see that the optimum is at $x_2^* = b/\sqrt{b^2 + c^2} = \beta/g_{21}$. For the cases depicted in Figs. 1 (a) and (b), we have $ab \leq b^2 + c^2$ and the solution lies on the line ax_2 . Therefore, we have $\gamma_2^* = (ax_2^*)^2$. In Fig. 1 (c), we have $ab > b^2 + c^2$ and the optimum lies on the curve $bx_2 + c\sqrt{1-x_2^2}$. Therefore, we have $\gamma_2^* = b^2 + c^2$. The interpretation is that TX₂ uses a beamforming vector in the direction of the crosstalk channel. Note that in Fig. 1, we depicted the scenario of $b > c$. The above analysis does not change if $b \leq c$. We summarize the solutions of (55)–(56) and (57) in the following proposition.

Proposition 2. *The optimal solution (x_1^*, y_1^*) of (55)–(56) is*

$$x_1^* = \max \left\{ 0, \frac{\alpha_1}{g_{11}^2} \sqrt{\gamma_1^* \sigma_1^2} - \frac{\tilde{\alpha}_1}{g_{11}^2} \sqrt{g_{11}^2 - \gamma_1^* \sigma_1^2} \right\}, \quad (60)$$

$$y_1^* = \left(\sqrt{\gamma_1^* \sigma_1^2} - \alpha_1 x_1^* \right) / \tilde{\alpha}_1. \quad (61)$$

Then, the optimal value of (45) is given as

$$\gamma_2^* = \begin{cases} \frac{g_{22}^2 (x_2^*)^2}{(x_1^* g_{11} g_{12})^2 + \sigma_2^2}, & a \leq b + c^2/b, \\ \frac{g_{21}^2}{\sigma_1^2 (\gamma_1^* + 1)}, & a > b + c^2/b \end{cases} \quad (62)$$

for

$$x_2^* = \begin{cases} 1, & a \leq b, \\ c/\sqrt{c^2 + (a-b)^2}, & b < a \leq b + c^2/b, \\ \beta_2/g_{21}, & a > b + c^2/b, \end{cases} \quad (63)$$

The optimal $(\mathbf{w}_1^*, \mathbf{w}_2^*)$ is obtained by inserting (60)–(61) and (63) into (47)–(48).

Prop. 2 provides a scheme for finding in closed-form a point on the Pareto boundary \mathcal{B}^{dn} , by providing γ_2^* as an explicit function of γ_1^* . In Tab. III, we summarize the proposed method for computing the entire \mathcal{B}^{dn} .

Contrary to the \mathcal{R}^{nm} case, we can obtain the weak, i.e., vertical and horizontal, parts of \mathcal{B}^{dn} by using the method in Tab. III. The reason is that by using the parameterization (47)–(48), we can set $p_i(\mathbf{w}_i) = 0$, which is not possible for \mathcal{R}^{nm} . Moreover, it is of interest to analyze the largest value, $\bar{\gamma}_2^{dn}$, that γ_2^* can assume, i.e., when $\gamma_1^* = 0$, since this brings some insight to \mathcal{R}^{dn} . At this point we have $a = g_{22}/\sigma_2$, $b = \beta_2/\sigma_1$, and $c = \tilde{\beta}_2/\sigma_1$. Therefore, for $\gamma_1^* = 0$ we have,

$$\bar{\gamma}_2^{dn} = \begin{cases} \frac{g_{22}^2}{\sigma_2^2}, & \frac{g_{22}}{\sigma_2} \leq \frac{\beta_2}{\sigma_1}, \\ \frac{\tilde{\beta}_2^2 g_{22}^2}{\beta_2^2 \sigma_2^2 + (g_{22} \sigma_1 - \beta_2 \sigma_2)^2}, & \frac{\beta_2}{\sigma_1} < \frac{g_{22}}{\sigma_2} \leq \frac{g_{21}}{\kappa_2 \sigma_1}, \\ \frac{g_{21}^2}{\sigma_1^2}, & \frac{g_{22}}{\sigma_2} > \frac{g_{21}}{\kappa_2 \sigma_1}. \end{cases} \quad (64)$$

Since $\beta_2 = \kappa_2 g_{21}$, the first case of (64) corresponds to the scenario where the crosstalk channel \mathbf{h}_{21} is strong compared to the direct channel \mathbf{h}_{22} and the spatial correlation between \mathbf{h}_{21} and \mathbf{h}_{22} is large. For this scenario, it is optimal for TX₂ to use the MR beamforming vector. The third case of (64) corresponds to the scenario where \mathbf{h}_{21} is weak compared to \mathbf{h}_{22} , and the spatial correlation between \mathbf{h}_{21} and \mathbf{h}_{22} is large.

For this case, TX₂ has to prioritize the SINR at RX₁ and it uses a beamforming vector in the direction of \mathbf{h}_{21} . The second case of (64) is somewhere in between the previous extreme cases. For this case, TX₂ chooses its beamforming vector such that both the RXs get the same SINR. To conclude, the highest rate link 2 can achieve in \mathcal{R}^{dn} is $\bar{R}_2^{dn} = \log_2(1 + \bar{\gamma}_2^{dn})$.

1:	Input and output: same as in Tab. I
2:	$\mathbf{r}_1 = \left[0 : \bar{R}_1^{dn}/(M-1) : \bar{R}_1^{dn} \right]$
3:	for $k = 1 : M$
4:	$\gamma_1^* = 2^{r_1(k)} - 1$
5:	Compute x_1^* and y_1^* using (60) and (61)
6:	Compute x_2^* using (63)
7:	Compute \mathbf{w}_1^* and \mathbf{w}_2^* using (47) and (48)
8:	Compute γ_2^* using (62)
9:	$\mathbf{r}_2(k) = R_2^* = \log_2(1 + \gamma_2^*)$
10:	end

TABLE III
CLOSED-FORM METHOD TO COMPUTE \mathcal{B}^{dn}

VI. BOTH RXS DECODE THE INTERFERENCE

In this section, we propose a computationally efficient numerical method to compute \mathcal{B}^{dd} which is similar in logic to the one given in Sec. IV-A for \mathcal{B}^{nm} and also utilizes intermediate results from the method in Sec. V for \mathcal{B}^{dn} . The method proposed herein improves the corresponding one of [2] in two ways: a) the number of variables is decreased from four real variables to a single one and b) a single instance of two quasi-concave subproblems needs to be solved instead of a sequence of convex feasibility problems.

Inserting the rate expressions (11) and (12) in the optimization problem (13)–(14) and equivalently reformulating the rate maximization to SINR maximization problem, we obtain

$$\begin{aligned} & \underset{(\mathbf{w}_1, \mathbf{w}_2) \in \mathcal{W}^2}{\text{maximize}} && \min \left\{ \frac{p_2(\mathbf{w}_2)}{\sigma_2^2}, \frac{q_1(\mathbf{w}_2)}{p_1(\mathbf{w}_1) + \sigma_1^2} \right\} && (65) \\ & \text{subject to} && p_1(\mathbf{w}_1)/\sigma_1^2 \geq \gamma_1^*, && (66) \end{aligned}$$

$$\frac{q_2(\mathbf{w}_1)}{p_2(\mathbf{w}_2) + \sigma_2^2} \geq \gamma_1^*, \quad (67)$$

where (66)–(67) follow from the epigraph formulation of (11), see [27, Ch. 3]. The formulation (65)–(67) is nonconvex, since the constraints are fractions of quadratic functions.

In [11], it was shown that the PO beamforming vectors of the \mathcal{R}^{dd} region can be parameterized as

$$\mathbf{w}_i(x_i, y_i) = x_i \frac{\mathbf{\Pi}_{\mathbf{h}_{ii}} \mathbf{h}_{ij}}{\|\mathbf{\Pi}_{\mathbf{h}_{ii}} \mathbf{h}_{ij}\|} + y_i \frac{\mathbf{\Pi}_{\mathbf{h}_{ii}}^\perp \mathbf{h}_{ij}}{\|\mathbf{\Pi}_{\mathbf{h}_{ii}}^\perp \mathbf{h}_{ij}\|} \quad (68)$$

for $i, j = 1, 2$ and $j \neq i$, where $(x_i, y_i) \in \mathcal{Q}$. Note that this parameterization is different from (19) and (39) of \mathcal{R}^{nm} and (47)–(48) of \mathcal{R}^{dn} . Inserting (68) into (2), we get

$$p_i(\mathbf{w}_i) = x_i^2 \frac{|\mathbf{h}_{ii}^H \mathbf{h}_{ij}|^2}{\|\mathbf{\Pi}_{\mathbf{h}_{ii}} \mathbf{h}_{ij}\|^2} = g_{ii}^2 x_i^2, \quad (69)$$

$$q_i(\mathbf{w}_j) = \left(x_j \|\mathbf{\Pi}_{\mathbf{h}_{jj}} \mathbf{h}_{ji}\| + y_j \|\mathbf{\Pi}_{\mathbf{h}_{jj}}^\perp \mathbf{h}_{ji}\| \right)^2$$

$$= (\beta_j x_j + \tilde{\beta}_j y_j)^2, \quad (70)$$

where the parameters $g_{ii}, \beta_i, \tilde{\beta}_j$ are defined in Sec. II. From (68), we see that the PO beamforming vectors of both TXs do not necessarily use all available power. However, without loss of optimality, we can assume that full power is used at optimum. This is so because increasing y_i increases the interference (70) but does not affect the desired signal power (69). The effect of increasing y_i , beyond the optimal solution y_i^* , is to only make the constraint (67) looser at optimum, without decreasing the objective value (65). The interpretation is that we can increase the interference arbitrarily, since it will be canceled by the RXs. Hence, we can increase it until the power constraint is met with equality, i.e., set $y_i = \sqrt{1 - x_i^2}$.

Inserting (69)–(70) in (65)–(67), taking the square root of objective and constraints, and introducing the nonnegative auxiliary variable z , we equivalently obtain

$$\begin{aligned} & \underset{0 \leq x_1, x_2 \leq 1, z \geq 0}{\text{maximize}} && z \end{aligned} \quad (71)$$

$$\text{subject to} \quad g_{22}x_2/\sigma_2 \geq z, \quad (72)$$

$$\frac{\beta_2 x_2 + \tilde{\beta}_2 \sqrt{1 - x_2^2}}{\sqrt{g_{11}^2 x_1^2 + \sigma_1^2}} \geq z, \quad (73)$$

$$g_{11}x_1/\sigma_1 \geq \sqrt{\gamma_1^*}, \quad (74)$$

$$\frac{\beta_1 x_1 + \tilde{\beta}_1 \sqrt{1 - x_1^2}}{\sqrt{g_{22}^2 x_2^2 + \sigma_2^2}} \geq \sqrt{\gamma_1^*}. \quad (75)$$

In order to further simplify the notation, we define

$$\tilde{u}_i(x_i) \triangleq \beta_i x_i + \tilde{\beta}_i \sqrt{1 - x_i^2}, \quad (76)$$

$$\tilde{v}_i(x_i) \triangleq \sqrt{g_{ii}^2 x_i^2 + \sigma_i^2}. \quad (77)$$

Problem (71)–(75) is feasible for $\gamma_1^* \in [0, \bar{\gamma}_1^{dd}]$. The rate $\bar{R}_1^{dd} = \log_2(1 + \bar{\gamma}_1^{dd})$ is the highest rate of link TX₁ → RX₁ that can be decoded by both RXs, achieved when TX₂ does not transmit. We determine $\bar{\gamma}_1^{dd}$ as

$$\bar{\gamma}_1^{dd} = \left(\underset{0 \leq x_1 \leq 1}{\text{maximize}} \min \left\{ \frac{g_{11}x_1}{\sigma_1}, \frac{\beta_1 x_1 + \tilde{\beta}_1 \sqrt{1 - x_1^2}}{\sigma_2} \right\} \right)^2. \quad (78)$$

The maximization in (78) is similar to (58), so we can solve it using (64). By interchanging the indices in (78), we can find $\bar{\gamma}_2^{dd}$.

Due to the variable z , (73) does not define a convex set. Hence, (71)–(75) is neither a concave nor a quasi-concave problem as it stands. But, by using the epigraph formulation, (71)–(75) can be equivalently reformulated into a quasi-concave problem. By studying the KKT conditions of (71)–(75), we identify two cases and apply to each of them techniques introduced in Secs. IV-A and V, respectively. The fact that the gradient of the Lagrange function of (71)–(75) vanishes at the optimum, gives the KKT conditions

$$\frac{\partial \mathcal{L}}{\partial z} = 1 - \mu_1 - \mu_2 = 0, \quad (79)$$

$$\frac{\partial \mathcal{L}}{\partial x_1} = -\mu_2 \frac{\tilde{v}'_1(x_1) \tilde{u}_2(x_2)}{\tilde{v}_1^2(x_1)} + \mu_3 \frac{g_{11}}{\sigma_1} + \mu_4 \frac{\tilde{u}'_1(x_1)}{\tilde{v}_2(x_2)} = 0, \quad (80)$$

$$\frac{\partial \mathcal{L}}{\partial x_2} = \mu_1 \frac{g_{22}}{\sigma_2} + \mu_2 \frac{\tilde{u}'_2(x_2)}{\tilde{v}_1(x_1)} - \mu_4 \frac{\tilde{v}'_2(x_2) \tilde{u}_2(x_2)}{\tilde{v}_2^2(x_2)} = 0, \quad (81)$$

where $\mu_i \geq 0$, $i \in \{1, 2, 3, 4\}$ are the Lagrange multipliers of constraints (72)–(75), respectively. First, we observe that we can have $\mu_3 = \mu_4 = 0$ only when $x_1 = 0$. This is the case only when $\gamma_1^* = 0$. Hence, for every other point we have either $\mu_3 > 0$ or $\mu_4 > 0$, corresponding to equality in (74) and (75), respectively. Next, for each case, we change the corresponding inequality in (71)–(75) to equality. We solve the two programs separately and compare the solutions. The solution with the highest optimal value will yield the optimum of (71)–(75).

For the case of equality in (74), it immediately follows that $x_1^* = \sqrt{\gamma_1^* \sigma_1^2 / g_{11}^2}$. From (75), we see that the problem is feasible only if $\beta_1 x_1^* + \tilde{\beta}_1 \sqrt{1 - (x_1^*)^2} \geq \sqrt{\gamma_1^* \sigma_2^2}$. Note that this is always the case if $\gamma_1^* \leq \bar{\gamma}_1^{dd}$. Given that (71)–(75) is feasible with equality in (74), we have the problem

$$\underset{0 \leq x_2 \leq 1}{\text{maximize}} \quad \min \left\{ \frac{g_{22}x_2}{\sigma_2}, \frac{\tilde{u}_2(x_2)}{\sqrt{\gamma_1^* + \sigma_1^2}} \right\} \quad (82)$$

$$\text{subject to} \quad x_2 \leq \frac{1}{g_{22} \sqrt{\gamma_1^*}} \sqrt{\tilde{u}_1^2(x_1^*) - \gamma_1^* \sigma_2^2}. \quad (83)$$

Note that x_2 is real and non-negative whenever the structure of (82)–(83) is similar to (57). The only difference is the extra constraint (83) which yields a tighter upper bound for x_2 . Hence, we can use Prop. 2 to find x_2^* by using coefficients $\tilde{a} \triangleq g_{22}/\sigma_2$, $\tilde{b} \triangleq \beta_2/\sqrt{\gamma_1^* + \sigma_1^2}$, and $\tilde{c} \triangleq \tilde{\beta}_2/\sqrt{\gamma_1^* + \sigma_1^2}$, in place of a , b , and c , respectively.

For the case of equality in (75), we get

$$x_2 = \frac{1}{g_{22} \sqrt{\gamma_1^*}} \sqrt{\tilde{u}_1^2(x_1) - \gamma_1^* \sigma_2^2} \triangleq \tilde{w}(x_1). \quad (84)$$

Inserting (84) in (71)–(75) yields the problem

$$\underset{0 \leq x_1 \leq 1}{\text{maximize}} \quad \min \{s_1(x_1), s_2(x_1)\} \quad (85)$$

$$\text{subject to} \quad g_{11}x_1/\sigma_1 \geq \sqrt{\gamma_1^*}, \quad (86)$$

$$\tilde{u}_1(x_1) \geq \sqrt{\gamma_1^* \sigma_2^2}, \quad (87)$$

$$\tilde{u}_1(x_1) \leq \sqrt{\gamma_1^* (g_{22}^2 + \sigma_2^2)}, \quad (88)$$

where

$$s_1(x_1) \triangleq g_{22} \tilde{w}(x_1) / \sigma_2, \quad (89)$$

$$s_2(x_1) \triangleq \tilde{u}_2(\tilde{w}(x_1)) / \tilde{v}_1(x_1). \quad (90)$$

The constraints (87) and (88) correspond to $x_2 \geq 0$ and $x_2 \leq 1$, respectively. Constraint (86) is satisfied if $g_{11}/\sigma_1 \geq \sqrt{\gamma_1^*}$, constraint (87) is satisfied if $\tilde{u}_1(\kappa_1) = g_{12}^2 \geq \sqrt{\gamma_1^* \sigma_2^2}$ and constraint (88) is satisfied if $\tilde{u}_1(0) = \tilde{\beta}_1 \leq \sqrt{\gamma_1^* (g_{22}^2 + \sigma_2^2)}$. Hence, (85)–(88) is feasible when

$$\frac{(1 - \kappa_1^2) g_{12}^2}{g_{22}^2 + \sigma_2^2} \leq \gamma_1^* \leq \min \left\{ \frac{g_{11}^2}{\sigma_1^2}, \frac{g_{12}^2}{\sigma_2^2} \right\}. \quad (91)$$

By comparing the RHS of (91) with (78), we see that $\bar{\gamma}_1^{dd} \leq \min\{g_{11}^2/\sigma_1^2, g_{12}^2/\sigma_2^2\}$. While (82)–(83) is feasible for all $\gamma_1^* \leq \bar{\gamma}_1^{dd}$, the optimization (85)–(88) is feasible only for a smaller subset as already illustrated by (91). The optimization (85)–(88) will be solved using a method similar to that used

for solving (29) for \mathcal{B}^{dd} in Sec. IV-A. First, we show that we do not need to solve (85)–(88) for all γ_1^* satisfying (91). By revisiting the KKT conditions (79)–(81), we see that if $\mu_4 > 0$ and $x_1 > \kappa_1$, then we must have $\mu_3 > 0$ as well. This follows since $\tilde{u}'_1(x_1) < 0$ for $x_1 > \kappa_1$. But the case of $\mu_3 > 0$ is already covered by (82)–(83). Hence, if $\gamma_1^* > g_{11}^2 \kappa_1^2 / \sigma_1^2$, it suffices to solve (82)–(83) and we set the optimal value of (85)–(88) to zero. Therefore, in the following, we only consider the upper bound $\gamma_1^* \leq g_{11}^2 \kappa_1^2 / \sigma_1^2$ and lower bound of (91). Second, we determine upper and lower bounds on x_1 . Since $\tilde{u}_1(x_1)$ is non-decreasing for $x_1 \leq \kappa_1$, the constraint yields an upper bound on the optimal x_1 ; namely $x_1 \leq \bar{x}_1$, where

$$\bar{x}_1 \triangleq \begin{cases} \kappa_1 \sqrt{\frac{\gamma_1^*}{\tilde{\gamma}_1^{\text{MR}}} - \sqrt{1 - \kappa_1^2}} \sqrt{1 - \frac{\gamma_1^*}{\tilde{\gamma}_1^{\text{MR}}}}, & \gamma_1^* \leq \tilde{\gamma}_1^{\text{MR}}, \\ \kappa_1, & \gamma_1^* > \tilde{\gamma}_1^{\text{MR}}, \end{cases} \quad (92)$$

where $\tilde{\gamma}_1^{\text{MR}} \triangleq g_{12}^2 / (g_{22}^2 + \sigma_2^2)$ is the SINR at RX₂ when it decodes the interference while TX₁ and TX₂ transmit in the MR directions of \mathbf{h}_{12} and \mathbf{h}_{22} , respectively. The constraints (86) and (87) yield a lower bound $x_1 \geq \underline{x}_1$, where

$$\underline{x}_1 \triangleq \max \left\{ \frac{\sqrt{\gamma_1^* \sigma_1^2}}{g_{11}}, \kappa_1 \sqrt{\frac{\sigma_2^2 \gamma_1^*}{g_{12}^2}} - \sqrt{1 - \kappa_1^2} \sqrt{1 - \frac{\sigma_2^2 \gamma_1^*}{g_{12}^2}} \right\}. \quad (93)$$

Next, we show that the objective function (85) is quasi-concave for $x_1 \in [\underline{x}_1, \bar{x}_1]$. We note that the minimum of two quasi-concave functions is quasi-concave [27, Ch. 3.4]. The function (89) is on the same form as (26) and hence, it is concave. So, if (90) is quasi-concave, then (85) is quasi-concave. We note that (90) has the same structure as the objective function of (29). Hence it follows from Lem. 2 that (90) is quasi-concave.

Since (85) is quasi-concave, we can use a gradient method similar to the respective one for \mathcal{B}^{nn} , presented in Tab. I. The proposed method to compute \mathcal{B}^{dd} is sketched in Tab. IV and differs in the following points to the one for \mathcal{B}^{nn} . First, for \mathcal{B}^{dd} we have to solve two optimization problems, which we do separately. We denote x_{11}^* , x_{21}^* and γ_{21}^* the optimal solution and value, respectively, of (82)–(83), and x_{12}^* , x_{22}^* and γ_{22}^* the optimal solution and value, respectively, of (85)–(88). The solution to the subproblem that yields the highest optimal value is declared the solution to (71)–(75). If both subproblems are infeasible, we set the optimal value to zero. Second, we maximize the minimum of two functions. Therefore, in lines 13–17, we let the gradient of the objective function (85), denoted by Δ , at a point x_1 , take as value the minimum of the derivatives of functions $s_1(x_1)$ and $s_2(x_2)$. In lines 21–22, we use $\tilde{s}(x_1) \triangleq \min \{s_1(x_1), s_2(x_1)\}$. Except for these points, the method works as for \mathcal{B}^{nn} .

VII. NUMERICAL ILLUSTRATIONS

Here we illustrate how the channel parameters g_{ij} , κ_i , $i, j = 1, 2$ affect the shape of the rate regions. By choosing these parameters in a controlled way, instead of randomly drawing channel vectors, we can illustrate interesting properties of the four rate regions. Also, we provide an analysis of

1:	Input and output: same as in Tab. I
2:	Output: \mathcal{B}^{dd} given by vectors $\mathbf{r}_1, \mathbf{r}_2 \in \mathbb{R}^M$
3:	$\mathbf{r}_1 = [0 : \bar{R}^{dd} / (M - 1) : \bar{R}_1^{dd}]$
4:	$\mathbf{r}_2(1) = \bar{R}_2^{dd}, x_1^* = 0$
5:	for $k = 2 : M$
6:	$\gamma_1^* = 2^{r_1(k)} - 1$
7:	Solve (82)–(83) using Prop. 2 $\Rightarrow x_{11}^*, x_{21}^*, \gamma_{21}^*$
8:	if $(1 - \kappa_1)^2 g_{12}^2 / (g_{22}^2 + \sigma_2^2) \leq \gamma_1^* \leq g_{11}^2 \kappa_1^2 / \sigma_1^2$
9:	Compute \bar{x}_1 and \underline{x}_1 using (92) and (93)
10:	$x_{12}^{(0)} = [x_{11}^* \bar{x}_1$
11:	$l = 0$
12:	repeat
13:	if $s_1(x_{12}^{(l)}) \leq s_2(x_{12}^{(l)})$
14:	$\Delta = s'_1(x_{12}^{(l)})$
15:	else
16:	$\Delta = s'_2(x_{12}^{(l)})$
17:	end
18:	Determine step size t
19:	$x_{12}^{(l+1)} = [x_{12}^{(l)} + t\Delta]_{\underline{x}_1}$
20:	$l \leftarrow l + 1$
21:	until $ \tilde{s}(x_{12}^{(l)}) - \tilde{s}(x_{12}^{(l-1)}) < \epsilon$
22:	$\gamma_{22}^* = \tilde{s}^2(x_{12}^{(l)})$
23:	Compute x_{22} using (84)
24:	else
25:	$\gamma_{22}^* = 0$
26:	end
27:	if $\gamma_{21}^* \geq \gamma_{22}^*$
28:	$\gamma_2^* = \gamma_{21}^*, x_1^* = x_{11}^*, x_2^* = x_{21}^*$
29:	else
30:	$\gamma_2^* = \gamma_{22}^*, x_1^* = x_{12}^*, x_2^* = x_{22}^*$
31:	end
32:	Compute \mathbf{w}_i^* using (68)
33:	Compute $\mathbf{r}_2(k) = R_2^* = \log_2(1 + \gamma_2^*)$
34:	end

TABLE IV
NUMERICAL METHOD TO COMPUTE \mathcal{B}^{dd}

the computational complexity of the proposed methods.

In Figs. 2–4, we illustrate the scenario where the channel gains are symmetric with $g_{11} = g_{22} = 1$ and $g_{12} = g_{21} = 2$. That is, the crosstalk channels are stronger than the direct channels. In Fig. 2, we have $\kappa_1 = \kappa_2 = 0.3$, which corresponds to a low spatial correlation of amongst the direct and crosstalk channels. We see that, even though the crosstalk channel gains are high, \mathcal{R}^{nn} is almost rectangular and all the other regions are contained in \mathcal{R}^{nn} . In this case, there is no need of cancel out interference; it costs too much in terms of useful signal power to create extra interference in order to enable interference cancellation.

We illustrate the other extreme case in Fig. 3. Here we have $\kappa_1 = \kappa_2 = 0.85$, which corresponds to the case where the angle between the direct and crosstalk channel vectors is small. We see that all the other regions are contained in \mathcal{R}^{dd} . The combination of strong crosstalk channels and high spatial

correlation, entails that the cost of boosting interference in order enable interference cancellation is very small.

In Fig. 4, we depict the case of $\kappa_1 = 0.85$ and $\kappa_2 = 0.3$, i.e., the channels from TX₁ and TX₂ have high and low spatial correlation, respectively. In this case we have $\mathcal{R} = \mathcal{R}^{nd}$. The reason is that RX₂ experiences high interference and has no problem to decode it. On the other hand RX₁ experiences low interference, so it is better to treat it as noise.

For both Fig. 2 and Fig. 4, we see that $\mathcal{R}^{dd} \subseteq \mathcal{R}^{dn} \cup \mathcal{R}^{nd}$. This is something that we frequently observe when the channels are i.i.d. Rayleigh and SNR is around 0 dB. The explanation is that for \mathcal{R}^{dd} both links have to sacrifice part of the desired signal power in order to enable interference cancellation.

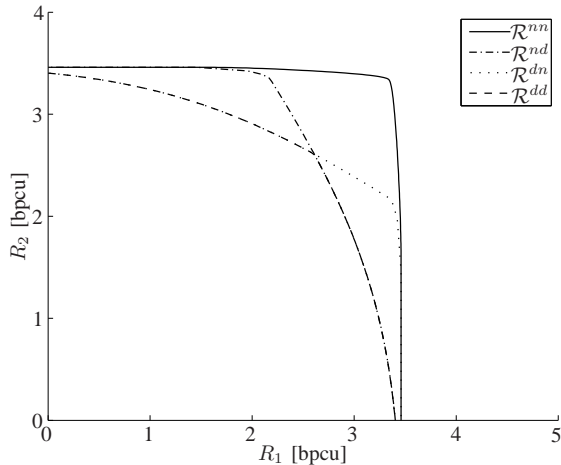


Fig. 2. Rate regions for $g_{11} = g_{22} = 1$, $g_{12} = g_{21} = 2$, $\kappa_1 = \kappa_2 = 0.3$

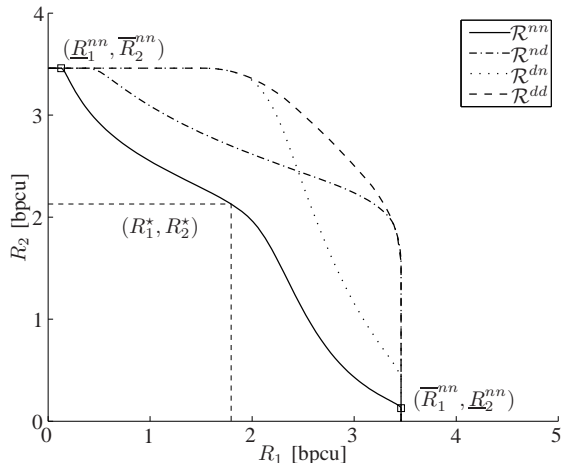


Fig. 3. Rate regions for $g_{11} = g_{22} = 1$, $g_{12} = g_{21} = 2$, $\kappa_1 = \kappa_2 = 0.85$

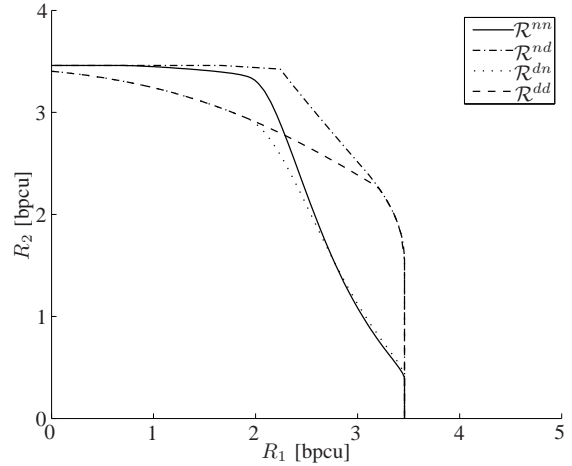


Fig. 4. Rate regions for $g_{11} = g_{22} = 1$, $g_{12} = g_{21} = 2$, $\kappa_1 = 0.85$, $\kappa_2 = 0.3$

A. Computational Complexity

Here, we consider the computational complexity of the proposed methods. We give both order expressions and the number of flops required to find the boundaries for the regions in Figs. 2–4. In Tab. V, we compare the complexity of the proposed methods with that of the brute-force methods.

The complexity of the proposed methods depends on the number of grid points, M , of each parameter. For the closed-form method for \mathcal{B}^{nn} given in Sec. IV-B, the parameter is λ_1^* . For the other three methods, the parameter is γ_1^* . From the descriptions of the methods given in Tabs. I–IV it is clear that all four methods have a computational complexity of $\mathcal{O}(M)$ flops. The brute-force method for \mathcal{B}^{nn} is based on a search over a two-dimensional parameter space [13]. We get M^2 rate points when we sample each parameter in M grid points. The algorithm⁸ we use to find the boundary out of L rate pairs is similar to the mergesort algorithm, see e.g., [30], which has a worst-case complexity of $\mathcal{O}(L \log L)$ flops. Hence, the total complexity of the brute-force comparison is $\mathcal{O}(M^2 \log M)$ flops. For \mathcal{B}^{dn} and \mathcal{B}^{nd} , we need three parameters to describe all pairs of potentially PO points [12]. Hence, the search is over M^3 rate points and the total complexity is $\mathcal{O}(M^3 \log M)$ flops. For \mathcal{B}^{dd} , we need four parameters according to [12], which would imply a total complexity of $\mathcal{O}(M^4 \log M)$ flops. On the other hand, we noticed in Sec. VI that it is straightforward to reduce the number of parameters to two and the total complexity to $\mathcal{O}(M^2 \log M)$ flops.

In Tab. V, we give the complexities for the proposed methods and the brute-force methods. In the numerical computations, we use $M = 500$ grid points and the tolerance $\epsilon = 5.0 \cdot 10^{-5}$. The complexity for computing the channel constants g_{ij} , κ_i , σ_i^2 , $i, j = 1, 2$, and the final beamforming vectors is not included in this analysis. When we count the flops, we use the numbers given by [31]. The complexities of the proposed methods are at least one order-of-magnitude less than the corresponding brute-force methods. For \mathcal{B}^{dn}

⁸See the source code available at <http://urn.kb.se/resolve?urn=urn:nbn:se:liu:diva-93845>.

and \mathcal{B}^{nd} , the complexity reduces more than four orders-of-magnitude. The complexity of our closed-form method for \mathcal{B}^{nn} is about 20% less than the complexity of the method presented in [20]. This gain arises from the fact that our choice of parameterization of the beamforming vectors is more computationally efficient, which shows that the choice of parameterization is not unimportant. Also, the numerical method for \mathcal{B}^{nn} has 2–5 times higher complexity than the closed-form method. On the other hand, the numerical method is more efficient for solving (17)–(18) for a specific γ_1^* . For \mathcal{B}^{dd} , the gain is one order-of-magnitude. Compared to the state-of-the-art brute-force method with four parameters [12], which has complexity $\mathcal{O}(M^4 \log M)$ the gain is even larger. On a desktop computer running Matlab, it takes about 50 ms to find the boundaries of the four regions using the proposed methods. Using the brute-force methods, it takes a few hours to find the boundaries. One observation is that the numerical method for \mathcal{B}^{dd} is less complex than the numerical method for \mathcal{B}^{nn} . This might seem counterintuitive since (85)–(88) is more involved than (29), but the reason is that we partly solve the former in closed form.

	Order	Fig. 2	Fig. 3	Fig. 4
\mathcal{B}^{nn} , numerical, Tab. I	$\mathcal{O}(M)$	$2.3 \cdot 10^5$	$2.9 \cdot 10^5$	$5.1 \cdot 10^5$
\mathcal{B}^{nn} , closed-form, Tab. II	$\mathcal{O}(M)$	$1.0 \cdot 10^5$	$1.0 \cdot 10^5$	$1.0 \cdot 10^5$
\mathcal{B}^{nn} , closed-form, [20]	$\mathcal{O}(M)$	$1.3 \cdot 10^5$	$1.3 \cdot 10^5$	$1.3 \cdot 10^5$
\mathcal{B}^{nn} , brute-force, (19)	$\mathcal{O}(M^2 \log M)$	$4.2 \cdot 10^6$	$4.3 \cdot 10^6$	$4.4 \cdot 10^6$
\mathcal{B}^{dn} , closed-form, Tab. III	$\mathcal{O}(M)$	$7.0 \cdot 10^4$	$6.7 \cdot 10^4$	$7.0 \cdot 10^4$
\mathcal{B}^{dn} , brute-force, (47)–(48)	$\mathcal{O}(M^3 \log M)$	$8.8 \cdot 10^8$	$8.8 \cdot 10^8$	$8.8 \cdot 10^8$
\mathcal{B}^{nd} , closed-form, Tab. III	$\mathcal{O}(M)$	$7.0 \cdot 10^4$	$6.7 \cdot 10^4$	$6.8 \cdot 10^4$
\mathcal{B}^{nd} , brute-force, (47)–(48)	$\mathcal{O}(M^3 \log M)$	$8.8 \cdot 10^8$	$8.8 \cdot 10^8$	$8.8 \cdot 10^8$
\mathcal{B}^{dd} , numerical, Tab. IV	$\mathcal{O}(M)$	$8.8 \cdot 10^4$	$2.2 \cdot 10^5$	$1.2 \cdot 10^5$
\mathcal{B}^{dd} , brute-force, (68)	$\mathcal{O}(M^2 \log M)$	$2.2 \cdot 10^6$	$2.2 \cdot 10^6$	$2.0 \cdot 10^6$

TABLE V
COMPUTATIONAL COMPLEXITY IN FLOPS FOR THE EXAMPLES IN
FIGS. 2–4 FOR THE PROPOSED AND BRUTE-FORCE METHODS WITH
 $M = 500$.

VIII. CONCLUSION

We proposed an efficient method to compute the Pareto boundary of the rate region for the two-user MISO IC with SIC-capable RXs. The merit of the proposed method, compared to the state-of-the-art, is that it avoids the brute-force search over all potentially PO beamforming vector pairs. The complexity of the proposed method is constant with respect to the number of transmit antennas. More importantly, we observed that the complexity gain of the proposed methods is a few orders-of-magnitude compared to the state-of-the-art brute-force methods. We achieved this by solving the quasi-concave optimization either by solving a cubic equation or performing a scalar line search. Finally, the numerical results illustrate that SIC should be performed when the cost of boosting the interference is small, i.e., when the crosstalk channel is strong or the spatial correlation of the forward and crosstalk channels is large.

It appears unlikely that there is any structure left in the problem that we can exploit in order to further improve the efficiency. Unfortunately, it seems that the proposed methods are not directly applicable for the general K -user MISO IC,

where the number of parameters grows as $K(K-1)$ for \mathcal{R}^{nn} [14] and probably even faster for the other regions. The number of regions, corresponding to all possible decoding orders grows at least as $\mathcal{O}(((K-1)!)^K)$. This number follows from the case where each receiver decodes all $(K-1)$ interfering signals, which can be done in $(K-1)!$ different orders.

The practical usefulness of our methods has been demonstrated by studies by others. For example, the closed-form method for computing \mathcal{B}^{nn} was used in [32] for a system-level assessment of inter-operator spectrum sharing. Also, we can use the method for the MISO broadcast channel. However, for this task we have to perform an extra line search to find the optimal power allocation. Perhaps, the methodology we brought forward here can be applied to other problems too.

ACKNOWLEDGMENT

We would like to thank the associate editor and the three anonymous reviewers for their valuable comments that helped us to improve this paper.

REFERENCES

- [1] J. Lindblom, E. Karipidis, and E. G. Larsson, "Closed-form parameterization of the Pareto boundary for the two-user MISO interference channel," in *Proc. IEEE Int. Conf. on Acoustics, Speech, and Signal Process. (ICASSP)*, Prague, Czech Republic, May 2011, pp. 3372–3375.
- [2] —, "Efficient computation of the Pareto boundary for the two-user MISO interference channel with multi-user decoding capable receivers," in *Proc. IEEE Int. Workshop on Computational Advances in Multi-Sensor Adaptive Process. (CAMSAP)*, San Juan, Puerto Rico, Dec. 2011, pp. 241–244.
- [3] S. Vishwanath and S. A. Jafar, "On the capacity of the vector Gaussian interference channel," in *Proc. IEEE Inf. Theory Workshop (ITW)*, San Antonio, TX, Oct. 2004, pp. 365–369.
- [4] A. Carleial, "Interference channels," *IEEE Trans. Inf. Theory*, vol. 24, pp. 60–70, Jan. 1978.
- [5] H. Sato, "The capacity of the Gaussian interference channel under strong interference," *IEEE Trans. Inf. Theory*, vol. 27, no. 6, pp. 786–788, Jun. 1981.
- [6] T. Han and K. Kobayashi, "A new achievable rate region for the interference channel," *IEEE Trans. Inf. Theory*, vol. 27, no. 1, pp. 49–60, Jan. 1981.
- [7] M. H. M. Costa, "On the Gaussian interference channel," *IEEE Trans. Inf. Theory*, vol. 31, no. 5, pp. 607–615, Sep. 1985.
- [8] A. S. Motahari and A. K. Khandani, "Capacity bounds for the Gaussian interference channel," *IEEE Trans. Inf. Theory*, vol. 55, no. 2, pp. 620–643, Feb. 2009.
- [9] V. S. Annapureddy and V. V. Veeravalli, "Sum capacity of MIMO interference channels in the low interference regime," *IEEE Trans. Inf. Theory*, vol. 57, no. 5, pp. 2565–2581, May 2011.
- [10] H. Dahrouj and W. Yu, "Multicell interference mitigation with joint beamforming and common message decoding," *IEEE Trans. Commun.*, vol. 59, pp. 2264–2273, Aug. 2011.
- [11] K. M. Ho, D. Gesbert, E. Jorswieck, and R. Mochaourab, "Beamforming on the MISO interference channel with multi-user decoding capability," in *Proc. IEEE Asilomar Conf. Signals, Systems, and Computers*, Pacific Grove, CA, Nov 2010, pp. 1196–1201.
- [12] —, "Beamforming on the MISO interference channel with multi-user decoding capability," *IEEE Trans. Inf. Theory*, 2011, submitted. Available: <http://arxiv.org/abs/1107.0416>.
- [13] E. A. Jorswieck, E. G. Larsson, and D. Danev, "Complete characterization of the Pareto boundary for the MISO interference channel," *IEEE Trans. Signal Process.*, vol. 56, pp. 5292–5296, Oct. 2008.
- [14] R. Mochaourab and E. A. Jorswieck, "Optimal beamforming in interference networks with perfect local channel information," *IEEE Trans. Signal Process.*, vol. 59, pp. 1128–1141, Mar. 2011.
- [15] R. Zakhour and D. Gesbert, "Distributed multicell-miso precoding using the layered virtual sinr framework," *IEEE Trans. Wireless Commun.*, vol. 9, no. 8, pp. 2444–2448, Aug. 2010.

- [16] R. Zhang and S. Cui, "Cooperative interference management in multi-cell downlink beamforming," *IEEE Trans. Signal Process.*, vol. 58, pp. 5450–5458, Oct. 2010.
- [17] X. Shang, B. Chen, and H. V. Poor, "Multiuser MISO interference channels with single-user detection: Optimality of beamforming and the achievable rate region," *IEEE Trans. Inf. Theory*, vol. 57, pp. 4255–4273, Jul. 2011.
- [18] Y.-F. Liu, Y.-H. Dai, and Z.-Q. Luo, "Coordinated beamforming for MISO interference channel: Complexity analysis and efficient algorithms," *IEEE Trans. Signal Process.*, vol. 59, pp. 1142–1157, Mar. 2011.
- [19] R. Mochaourab and E. Jorswieck, "Walrasian equilibrium in two-user multiple-input single-output interference channels," in *Proc. IEEE Int. Conf. on Commun. (ICC)*, Kyoto, Japan, Jun. 2011, pp. 1–5.
- [20] —, "Exchange economy in two-user multiple-input single-output interference channels," *IEEE J. Sel. Topics Signal Process.*, vol. 6, no. 2, pp. 151–164, Apr. 2012.
- [21] E. Björnson, R. Zakhour, D. Gesbert, and B. Ottersten, "Cooperative multicell precoding: Rate region characterization and distributed strategies with instantaneous and statistical CSI," *IEEE Trans. Signal Process.*, vol. 58, no. 8, pp. 4298–4310, Aug. 2010.
- [22] E. G. Larsson and E. A. Jorswieck, "Competition versus cooperation on the MISO interference channel," *IEEE J. Sel. Areas Commun.*, vol. 26, pp. 1059–1069, Sep. 2008.
- [23] E. Karipidis and E. G. Larsson, "Efficient computation of the Pareto boundary of the MISO interference channel with perfect CSI," in *Proc. Int. Symp. on Modeling and Optimization in Mobile, Ad Hoc and Wireless Networks (WiOpt)*, Avignon, France, May 2010, pp. 573–577.
- [24] E. A. Jorswieck and E. G. Larsson, "Monotonic optimization framework for the two-user MISO interference channel," *IEEE Trans. Commun.*, vol. 58, no. 7, pp. 2159–2168, Jul. 2010.
- [25] E. Björnson and E. Jorswieck, "Optimal resource allocation in coordinated multi-cell systems," *Foundations and Trends in Communications and Information Theory*, vol. 9, no. 2–3, pp. 113–381, 2013.
- [26] D. G. Luenberger, *Microeconomic Theory*. McGraw-Hill, 1995.
- [27] S. Boyd and L. Vandenberghe, *Convex Optimization*. Cambridge University Press, 2004.
- [28] K. J. Arrow and A. C. Enthoven, "Quasi-concave programming," *Econometrica*, vol. 29, no. 4, pp. 779–800, Oct. 1961.
- [29] M. Abramowitz and I. A. Stegun, *Handbook of Mathematical Functions with Formulas, Graphs, and Mathematical Tables*. National Bureau of Standards, 1972.
- [30] D. E. Knuth, *Sorting and Searching*, ser. The Art of Computer Programming. Addison-Wesley, 1998, vol. 3.
- [31] T. Minka, "The Lightspeed Matlab Toolbox, version 2.6," <http://research.microsoft.com/en-us/um/people/minka/software/lightspeed>, May 2011.
- [32] R. Litjens, H. Zhang, I. Noppen, L. Yu, E. Karipidis, and K. Börner, "System-level assessment of non-orthogonal spectrum sharing via transmit beamforming," in *Proc. IEEE Veh. Tech. Conf. (VTC)*, Dresden, Germany, Jun. 2013.